

Role of an apical K_{Cl} cotransporter in urine formation by renal tubules of the yellow fever mosquito (*Aedes aegypti*)

Peter M. Piermarini, Rebecca M. Hine, Matthew Schepel, Jeremy Miyauchi, and Klaus W. Beyenbach

Department of Biomedical Sciences, Cornell University, Ithaca, New York

Submitted 27 April 2011; accepted in final form 29 July 2011

Piermarini PM, Hine RM, Schepel M, Miyauchi J, Beyenbach KW. Role of an apical K_{Cl} cotransporter in urine formation by renal tubules of the yellow fever mosquito (*Aedes aegypti*). *Am J Physiol Regul Integr Comp Physiol* 301: R1318–R1337, 2011. First published August 3, 2011; doi:10.1152/ajpregu.00223.2011.—The K_{Cl} cotransporters (KCCs) of the SLC12 superfamily play critical roles in the regulation of cell volume, concentrations of intracellular Cl⁻, and epithelial transport in vertebrate tissues. To date, the role(s) of KCCs in the renal functions of mosquitoes and other insects is less clear. In the present study, we sought molecular and functional evidence for the presence of a KCC in renal (Malpighian) tubules of the mosquito *Aedes aegypti*. Using RT-PCR on *Aedes* Malpighian tubules, we identified five alternatively spliced partial cDNAs that encode putative SLC12-like KCCs. The majority transcript is AeKCC1-A₁; its full-length cDNA was cloned. After expression of the AeKCC1-A protein in *Xenopus* oocytes, the Cl⁻-dependent uptake of ⁸⁶Rb⁺ is 1) activated by 1 mM N-ethylmaleimide and cell swelling, 2) blocked by 100 μM dihydroxyindenoxyalkanoic acid (DIOA), and 3) dependent upon N-glycosylation of AeKCC1-A. In *Aedes* Malpighian tubules, AeKCC1 immunoreactivity localizes to the apical brush border of principal cells, which are the predominant cell type in the epithelium. In vitro physiological assays of Malpighian tubules show that peritubular DIOA (10 μM): 1) significantly reduces both the control and diuretic rates of transepithelial fluid secretion and 2) has negligible effects on the membrane voltage and input resistance of principal cells. Taken together, the above observations indicate the presence of a KCC in the apical membrane of principal cells where it participates in a major electroneutral transport pathway for the transepithelial secretion of fluid in this highly electrogenic epithelium.

Malpighian tubules; SLC12; immunohistochemistry; *Xenopus* oocytes; fluid secretion

THE MALPIGHIAN TUBULE EPITHELIUM of mosquitoes secretes fluid containing Na⁺, K⁺, and Cl⁻ as the major osmolytes. Next to serving homeostatic functions of the extracellular fluid (hemolymph), the tubular fluid provides a compartment for the excretion of harmful organic solutes such as nitrogenous wastes and xenobiotics (5–7). The excretory functions of this renal epithelium are especially important to the hematophagous adult female mosquito after she has ingested a volume of blood that exceeds her own body mass (3, 12). The blood meal, which secures proteins and nutrients for developing eggs, presents significant challenges to the mosquito both physiologically (e.g., salt and volume loading) and ecologically (e.g., increased predation risk) (3, 6, 67). However, the prompt and potent diuresis mediated by Malpighian tubules, which commences while the mosquito is still feeding on blood, excretes

excess Na⁺, Cl⁻, and water, thereby lightening the flight payload and increasing the mosquito's chances of survival and successful reproduction (3, 6).

In the past few years, efforts in our laboratory have focused on identifying the molecular mechanisms that mediate the transepithelial secretion of fluid by Malpighian tubules of female mosquitoes (*Aedes aegypti*; *Aedes*, hereafter) (61, 62). We recently demonstrated that the enigmatic stellate cells of *Aedes* Malpighian tubules, which intercalate between the mitochondrion-rich principal cells, express a SLC4-like Cl/HCO₃⁻ anion exchanger (AeAE) in their basal membranes (61). The inhibition of this anion exchanger with the disulfonic stilbene derivative DIDS reduces diuretic rates, but not control rates, of fluid secretion in isolated *Aedes* Malpighian tubules (61). Thus, stellate cells appear to support the enhanced metabolic activity of neighboring principal cells during periods of diuretic fluid secretion, presumably by preventing the accumulation of metabolic HCO₃⁻ (6, 61).

To follow up on this putative metabolic support role of stellate cells during periods of heightened transepithelial electrolyte and fluid secretion, the present study sought to test the hypothesis that a K_{Cl} cotransporter (KCC), related to the SLC12 superfamily of electroneutral cation chloride cotransporters, is also present in the basal membrane of stellate cells where it might serve to maintain low intracellular concentrations of Cl⁻ for the optimal operation of AeAE. Our hypothesis is based on the known functional coupling in the basolateral membrane of type A intercalated cells of the mouse renal collecting tubule where KCC4 recycles Cl⁻ that is imported by the SLC4 transporter AE1 (9, 36).

To date, the presence of SLC12-like KCCs in insect Malpighian tubules is unclear and relies primarily on physiological measurements in isolated tubules. In brief, studies employing the KCC inhibitor dihydroxyindenoxyalkanoic acid (DIOA) have shown that this drug blocks the transepithelial secretion of fluid by Malpighian tubules of the hemipteran *Rhodnius prolixus* and the dipteran *Drosophila melanogaster* (24, 42). Likewise, in Malpighian tubules of the hymenopteran *Formica polyctena*, manipulation of the ionic composition of the peritubular Ringer solution indicated that a KCC-like transporter is functional under certain conditions (41). However, subsequent studies that measured electrochemical potentials for K⁺ and Cl⁻ in principal cells of Malpighian tubules in *Rhodnius* and *Drosophila* have indicated that the operation of KCCs in transepithelial fluid secretion is unlikely on thermodynamic grounds (33, 34).

In the present study, we demonstrate the expression of five alternatively spliced cDNAs encoding three distinct SLC12-like KCCs in *Aedes* Malpighian tubules (designated AeKCC1-A, -B, and -C). We show further that AeKCC1-A: 1) mediates DIOA-sensitive K⁺, Cl⁻ cotransport when expressed

Address for reprint requests and other correspondence: P. M. Piermarini, The Ohio State Univ., Ohio Agricultural Research and Development Center, Dept. of Entomology, 1680 Madison Ave., Wooster, OH 44691 (e-mail: piermarini.1@osu.edu).

heterologously in *Xenopus* oocytes, and 2) resides in the apical membrane of principal cells. Finally, physiological assays of isolated *Aedes* Malpighian tubules indicate that peritubular DIOA inhibits the transepithelial secretion of fluid without affecting the electrophysiological variables of principal cells. We conclude that an apical KCC serves as part of a transcellular, electroneutral transport pathway for the secretion of fluid by mosquito Malpighian tubules.

MATERIAL AND METHODS

Mosquitoes and Isolation of Malpighian Tubules

All mosquitoes (*A. aegypti*) used in this study were raised in the laboratory following the protocol of Pannabecker et al. (54), with the exception that the larval mosquitoes were fed finely ground TetraMin flakes (Melle, Germany). Malpighian tubules were isolated from cold-anesthetized, adult female mosquitoes (3–7 days posteclosion). In brief, after decapitating and removing the legs of a mosquito (with Dumont no. 5 fine forceps; Fine Science Tools, Foster City, CA), its body was submerged in a Ringer solution containing the following in mM: 150 NaCl, 3.4 KCl, 1.7 CaCl₂, 1.8 NaHCO₃, 1.0 MgSO₄, 5 glucose, and 25 HEPES (pH 7.1). The digestive tract was isolated by gently pulling on the rectal segment, and the five attached Malpighian tubules were removed with fine forceps. The isolated Malpighian tubules were used in the studies described below.

Cloning of K,Cl Cotransporter cDNAs from Aedes Malpighian Tubules

Basic local alignment search tool (BLAST) inquiries of the *Aedes* genome (52) with the amino acid sequences of mammalian KCCs revealed the presence of two genes that encode SLC12-like KCCs, which we designate as *AeKCC1* and *AeKCC2*. Neither gene was fully annotated in the available genomic databases (NCBI GenBank and Vectorbase), but a partial open-reading frame (ORF) for *AeKCC1* was associated with GenBank entry XM_001655694 (AAEL011792 in Vectorbase), and a partial ORF for *AeKCC2* was spread across two GenBank entries: XM_001662386 and XM_001662385 (AAEL012334 and AAEL012335 in Vectorbase). To ensure that cDNAs derived from both genes were detectable in our cloning efforts, the PCR primers used in the rapid amplification of cDNA ends (RACE) experiments (Table 1) were designed to conserved regions within the predicted ORFs of both *AeKCC* genes.

Using a Generacer Kit (Invitrogen, Carlsbad, CA), independent pools of 5' and 3' single-stranded cDNA were synthesized via reverse transcription (RT) from the total RNA extracted from ~150 Malpighian tubules (~30 females), as described previously (61). These

two pools of cDNA were used, respectively, as templates for the 5' and 3' RACE.

To enhance the sensitivity of the RACE experiments, a nested approach was followed as detailed in the Generacer Kit (Invitrogen). The initial 5'-RACE was conducted on Malpighian tubule 5'-cDNA using a 1) generic forward primer (GeneRacer 5'-Primer; Invitrogen); 2) *AeKCC* reverse primer (1R or 2R in Table 1); and 3) Platinum PCR Supermix HF (Invitrogen), following the touchdown thermocycling protocol of the Generacer Kit (Invitrogen). The nested 5'-RACE was performed on 0.5 µl of the initial 5'-RACE product using a 1) generic forward primer (GeneRacer Nested 5'-Primer; Invitrogen); 2) *AeKCC* reverse primer (3R in Table 1) that is upstream to primers 1R and 2R; and 3) Platinum PCR Supermix HF (Invitrogen), following the suggested nested thermocycling protocol of the Generacer Kit (Invitrogen).

The initial 3'-RACE was performed on Malpighian tubule 3'-cDNA using a 1) *AeKCC* forward primer (1F or 2F in Table 1); 2) generic reverse primer (GeneRacer 3'-Primer, Invitrogen); and 3) Platinum PCR Supermix HF (Invitrogen), following the same touchdown thermocycling protocol as above. The nested 3'-RACE was performed on 0.5 µl of the initial 3'-RACE product using a 1) *AeKCC* forward primer (3F or 4F in Table 1) that is downstream to primers 1F or 2F; 2) generic reverse primer (GeneRacer Nested 3'-Primer, Invitrogen); and 3) Platinum PCR Supermix HF (Invitrogen), following the same nested thermocycling protocol as above.

Products of the above PCRs were evaluated by agarose gel electrophoresis (with ethidium-bromide staining/UV transillumination), TA-cloned (Invitrogen), and chemically transformed into TOP10 *Escherichia coli* (Invitrogen). The resulting plasmid DNA was isolated from colonies of transformed *E. coli* and sequenced at the Cornell DNA Sequencing Center (Ithaca, NY), as described previously (61). After obtaining preliminary DNA sequences of the nested RACE products, it became apparent that the cloned cDNAs were derived from the *AeKCC1* gene and not the *AeKCC2* gene. Thus, the remaining cloning efforts focused on *AeKCC1*.

As will be presented in RESULTS (Fig. 1A), the 5'-RACE experiments detected the expression of five alternatively spliced partial cDNAs in *Aedes* Malpighian tubules. The partial cDNAs were designated as follows (GenBank accession no. in parentheses): *AeKCC1-A*₁ (JF958164), *AeKCC1-A*₂ (JF958165), *AeKCC1-B*₁ (JF958166), *AeKCC1-B*₂ (JF958167), and *AeKCC1-C* (JF958168). To estimate the relative abundance of the various splices, two approaches were employed. First, 112 colonies of *E. coli* that were transformed with TA-cloned 5'-RACE products were identified by DNA sequencing and/or by diagnostic PCR. Second, qualitative RT-PCRs on Malpighian tubule cDNA were conducted using pairs of gene-specific primers that bind to two possible splice variants of *AeKCC1*. These primers flank a region of 134 bp that is present or absent in certain splices (see dark gray region in Fig. 1A). Thus, the size of the PCR product is characteristic of the splice variant that is amplified. We used primers 5F and 2R (Table 1) to compare the abundances *AeKCC1-A* variants vs. *AeKCC1-B*₁, and used primers 6F and 2R (Table 1) to compare the abundances of *AeKCC1-B*₂ vs. *AeKCC1-C*.

After finding *AeKCC1-A*₁ as the most abundant transcript, its full-length cDNA was cloned from Malpighian tubule 5'-cDNA with primers 7F and 4R (Table 1), and Platinum PCR Supermix HF (Invitrogen) using the following cycling parameters: 1) one cycle at 94°C for 2 min; 2) 35 cycles at 94°C for 30 s, 65°C for 30 s, and 68°C for 5 min; and 3) one cycle at 68°C for 10 min. The PCR products were TA-cloned and sequenced as described above.

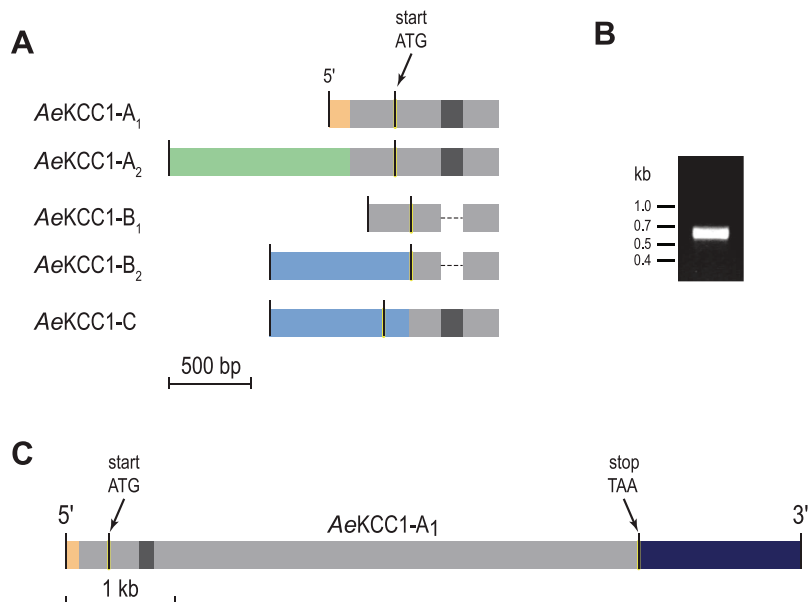
A consensus sequence for the entire *AeKCC1-A*₁ cDNA was generated via an assembly of DNA sequences obtained from the following *E. coli* colonies: 20 containing partial cDNAs derived from the 5'-RACE, four containing full-length cDNAs, and 10 containing partial cDNAs derived from the 3'-RACE. The consensus sequence was deposited to GenBank (accession no. HM125960).

Table 1. Primers used for cloning of *AeKCC* cDNAs

Name	Sequence (5'-3')	PCR reaction
1R	CCAGATACACGATCAGACCCATAAC	5'-RACE (initial)
2R	TTGTACATCGAGAACGCTTTCGT	5'-RACE (initial)
3R	CCAATATCGATAACCACGGACCAT	5'-RACE (nested)
4R	CGTTTGCTGCTGTGCCATCGTTACCG	Full-length
1F	GCCCCGCTGCTGTCCATGTCTTCTT	3'-RACE (initial)
2F	CTTTACCGTCGCCAGATGGAAGACAAT	3'-RACE (initial)
3F	GATGGCTCTGCTGTACCGAAGGGAAT	3'-RACE (nested)
4F	CGGCATACACCTACGAGCGAACCTGTAT	3'-RACE (nested)
5F	GCAGGTTGCTGCTCTCCGAGAAG	<i>AeKCC1-A</i> vs. -B ₁
6F	CCCAAATAAGGCTGTACCGGTGGAAC	<i>AeKCC1-C</i> vs. -B ₂
7F	AGTGGTGGATAGCGGGCGTTCAAGT	Full-length

AeKCC, *Aedes* K,Cl cotransporter; RACE, rapid amplification of cDNA ends.

Fig. 1. Cloning of alternatively spliced *AeKCC1* cDNAs. *A*: partial cDNAs cloned from adult female *Aedes* Malpighian tubules in the 5'-RACE experiments. Differences in nucleotide sequences are represented by different colors. The start of the predicted open-reading frame (ORF; start ATG) is indicated. Dashed horizontal lines indicate a region of 134 bp that is missing in the *AeKCC1*-B variants, but is present in the *AeKCC1*-A and *AeKCC1*-C variants (dark grey regions). Scale bar = 500 bp. *B*: qualitative RT-PCR in adult female *Aedes* Malpighian tubules using a gene-specific pair of primers designed to bind regions common to the *AeKCC1*-A variants and *AeKCC1*-B₁. A product of the size expected for *AeKCC1*-A₁ (~600 bp) is shown. *C*: full-length *AeKCC1*-A₁ cDNA cloned from Malpighian tubules. The start and stop of the predicted ORF (start ATG and stop TAA, respectively) are indicated. Scale bar = 1 kb.



Antibodies

Genscript USA (Piscataway, NJ) was hired to raise and affinity-purify a polyclonal rabbit antibody against a synthetic peptide that corresponds to a fragment of the cytosolic NH₂-terminal domain of the predicted *AeKCC1*-A and -C proteins (see green box in Fig. 6). This peptide (Glu³⁴-Lys⁴⁷) of *AeKCC1*-A is not found in the *AeKCC1*-B splice variant (Fig. 6). Efforts to raise antibodies that recognize a region that is conserved among all three of the predicted *AeKCC1* proteins were unsuccessful.

As in previous studies (61, 62), a monoclonal mouse antibody (JL-8) was purchased from Clontech (Mountain View, CA) to verify the heterologous expression of mosquito proteins fused to enhanced-green fluorescent protein (eGFP) in *Xenopus laevis* oocytes (see below).

Heterologous Expression of *AeKCC1*-A in *Xenopus Oocytes*

Generation of cDNA constructs and capped RNA. The entire ORF of *AeKCC1*-A was subcloned into a pGH19 plasmid (78). The resulting *AeKCC1*-A-pGH19 cDNA was then modified to include the ORF for eGFP at the 3'-end of the *AeKCC1*-A ORF (i.e., *AeKCC1*-A-eGFP-pGH19 cDNA), as described previously (62). The first construct encodes the native *AeKCC1*-A protein, whereas the second encodes an engineered *AeKCC1*-A-eGFP fusion protein.

The *AeKCC1*-A-eGFP-pGH19 cDNA was further modified to generate constructs containing mutations of the two putative N-glycosylation sites on the 5–6 loop: Asn²⁹⁸ and Asn³²⁵ (Figs. 4 and 5). In one construct (N298Q), the codon for Asn²⁹⁸ was changed to encode a Gln residue. Likewise, in another construct (N325Q), the codon for Asn³²⁵ was changed to encode a Gln residue. Finally, to generate a double-mutant construct (N298Q-N325Q), the N298Q construct was used as a template and the codon for Asn³²⁵ was changed to encode a Gln residue. The above changes were all made with the Quikchange site-directed mutagenesis kit (Stratagene; La Jolla, CA) according to the manufacturer's protocol and were verified by DNA sequencing.

Each of the generated cDNA constructs was used as a template to synthesize capped RNA (cRNA) with a T7 mMessage mMachine kit (Ambion; Austin, TX). The resulting cRNA was purified using an RNeasy MinElute Cleanup Kit (Qiagen) and stored in nuclease-free H₂O at -80°C.

Injection and culture of *Xenopus* oocytes. The *Xenopus* oocytes used in the present study were generously provided by the laboratory of Dr. William A. Horne (Cornell University, Ithaca, NY). The oocytes were isolated and prepared as described in previous studies (61, 62). To express a desired *AeKCC1*-A protein, oocytes were injected with 28 nl of the appropriate cRNA (1.0 ng/nl) and cultured in OR3 culture media for 5–10 days as described previously (61, 62). Oocytes injected with 28 nl of nuclease-free H₂O served as controls. In some cases, ~30 min before the injections of cRNA, the oocytes were injected with 2.5 ng of tunicamycin (MP Biomedicals, Solon, OH) or a comparable amount of 0.9% DMSO (Fisher Scientific, Hampton, NH), which is the tunicamycin vehicle.

To verify the heterologous expression of the *AeKCC1*-A-eGFP fusion proteins in *Xenopus* oocytes, Western blot analysis (with JL-8; 1 µg/ml) and/or *in vivo* fluorescence was used, as described previously (61, 62). The anti-*AeKCC1* antibody was used in Western blot analysis on both *AeKCC1*-A and *AeKCC1*-A-eGFP oocytes (Fig. 10).

Measurements of ⁸⁶Rb⁺ Uptake in *Xenopus Oocytes*

To functionally characterize *AeKCC1*-A expressed heterologously in *Xenopus* oocytes, we measured unidirectional uptake rates of ⁸⁶Rb⁺ (a congener of K⁺) following a procedure similar to that of Mount et al. (50). Note that only oocytes injected with *AeKCC1*-A cRNA or H₂O (5–10 days after injection) were used in the uptake experiments, because preliminary experiments indicated that the *AeKCC1*-A-eGFP fusion protein exhibited inferior functional activity relative to the native nontagged *AeKCC1*-A protein. A similar observation has been documented by another group that attempted to measure the functional activity of a SLC12-GFP fusion protein (32).

Solutions. The compositions of the solutions used in the uptake experiments are detailed in Table 2. Note that all solutions contain a minimal concentration of Na⁺ (~100 µM) and 0.5 mM ouabain that, respectively, limit the contributions of the endogenous oocyte Na₊K₊2Cl cotransporter and Na⁺/K⁺-ATPase to the uptake of ⁸⁶Rb⁺.

⁸⁶Rb⁺ uptake experiments. All of the following steps were performed at room temperature, unless noted otherwise. We used one of the four following protocols to characterize the uptake of ⁸⁶Rb⁺ mediated by *AeKCC1*-A. With the exception of the fourth protocol, H₂O-injected oocytes were run in parallel as controls.

The first protocol assessed the effects of N-ethylmaleimide (NEM) on the Cl⁻-dependent uptake of ⁸⁶Rb⁺. In brief, three groups of five

Table 2. Solutions used in $^{86}\text{Rb}^+$ uptake experiments

Solution	I	II	III	IV
NaCl	0	0	0.096	0.096
Na-Gluc	0.096	0.096	0	0
NMDG-Cl	0	0	48	48
NMDG-Gluc	48	48	0	0
KCl	0.07	0.07	2	2
K-Gluc	1.93	1.93	0	0
MgCl ₂	0	0	1	1
Mg-Gluc	2	2	0	0
CaCl ₂	0	0	1.8	1.8
Ca-Gluc	3.6	3.6	0	0
HEPES	5	5	5	5
Sucrose	95.8	0	95.8	0
Ouabain	0.5	0.5	0.5	0.5
Osmolality	200	100	200	100

All values are in mM, except for osmolality, which is in osmol/kgH₂O. The pH of all solutions was adjusted to 7.5 with NaOH or NMDG-OH. Before use, the osmolality of each solution was verified by vapor pressure osmometry. Gluc, gluconate; NMDG, *N*-methyl-D-glucammonium.

AeKCC1-A oocytes were distributed to separate wells of a 24-well polystyrene tissue-culture plate (BD Falcon, Franklin Lakes, NJ) filled with 2 ml of an isotonic low-Cl⁻ solution (*solution I*, Table 2). Following a brief incubation period of 5–10 min, each group of oocytes was transferred to a new well filled with one of the following preuptake solutions: 1) an isotonic high-Cl⁻ solution (*solution III*, Table 2), 2) an isotonic high-Cl⁻ solution containing 1 mM NEM, or 3) an isotonic low-Cl⁻ solution containing 1 mM NEM. After a 30-min preuptake period, each group was transferred to a new well containing 0.5 ml of the same respective preuptake solution supplemented with 2.5 μCi of $^{86}\text{RbCl}$ (PerkinElmer, Boston, MA), which initiated the uptake period. After a 60-min uptake period, 2 ml of an ice-cold isotonic low-Cl⁻ solution was added to each well, and the tissue-culture plate was placed on top of a frozen block of blue ice to maintain the cold temperature. Each group of oocytes was then transferred to a fresh well containing an ice-cold isotonic low-Cl⁻ solution and allowed to incubate for 5 min to wash the oocytes of any externally bound $^{86}\text{Rb}^+$. The wash step was repeated four times before scintillation counting (see *Cell lysis and scintillation counting* below).

The second protocol assessed the effects of cell swelling on the Cl⁻-dependent uptake of $^{86}\text{Rb}^+$. In brief, the NEM protocol described above was used with two modifications. First, the following preuptake solutions were used: 1) an isotonic high-Cl⁻ solution (*solution III*), 2) a hypotonic high-Cl⁻ solution (*solution IV*, Table 2), and 3) a hypotonic low-Cl⁻ solution (*solution II*, Table 2). Second, after the uptake period, each group of oocytes was washed with either an ice-cold isotonic low-Cl⁻ solution or an ice-cold hypotonic low-Cl⁻ solution to match the osmolality of the respective preuptake solutions.

The third protocol assessed the effects of DIOA (Sigma-Aldrich, St. Louis, MO) on the uptake of $^{86}\text{Rb}^+$. In brief, the cell-swelling protocol described above was used with the following preuptake solutions: 1) an isotonic high-Cl⁻ solution (*solution III*) containing 0.2% DMSO, 2) a hypotonic high-Cl⁻ solution (*solution IV*, Table 2) containing 0.2% DMSO, and 3) a hypotonic high-Cl⁻ solution containing DIOA (100 μM). DMSO is the vehicle for DIOA.

The fourth protocol compared the effects of DIOA, bumetanide, and furosemide (all from Sigma-Aldrich) on the uptake of $^{86}\text{Rb}^+$. In brief, this protocol is an expansion of the above DIOA protocol with the following changes. Five groups of *AeKCC1-A* oocytes were used instead of three. One of the five groups was transferred to a well filled with an isotonic high-Cl⁻ preuptake solution (*solution III*) containing 0.2% DMSO, while the remaining four groups were transferred to wells filled with a hypotonic high-Cl⁻ preuptake solution (*solution IV*) containing one of the following compounds: DMSO (0.2%),

DIOA (100 μM), bumetanide (100 μM), or furosemide (100 μM). DMSO is the vehicle for all of the inhibitors.

Cell lysis and scintillation counting. For the above protocols, each oocyte within a group was transferred to its own 7-ml glass scintillation vial (Fisher Scientific) containing 100 μl of 10% SDS (Fisher Scientific) to lyse the cell. Each vial was submitted to the following: 1) the addition of 6 ml of a liquid scintillation cocktail (ScintiSafe Econo2; Fisher Scientific), 2) vigorous shaking for 3–5 s, and 3) 2 min of β -scintillation counting on the wide channel (cat. no. LS6500; Beckman Coulter; Brea, CA). To obtain background readings, blank vials containing only the SDS and scintillation fluid were used.

Calculating the rates of $^{86}\text{Rb}^+$ influx. From the counts per minute emitted from each oocyte lysate, a rate of $^{86}\text{Rb}^+$ uptake (in fmol·oocyte⁻¹·h⁻¹) was calculated. First, the counts per minute values were converted to disintegrations per minute by correcting for the efficiency of the scintillation counter for $^{86}\text{Rb}^+$ (94%) and subtracting the background reading. Second, the disintegrations per minute values were converted to a Curie equivalent (2.22×10^{12} dpm per Curie). Finally, the Curie equivalent was divided by the specific activity (in Curies per mole $^{86}\text{Rb}^+$; provided by the supplier) to obtain the number of moles of $^{86}\text{Rb}^+$ per oocyte that were accumulated during the 1-h uptake period.

Western Blot Analysis of Malpighian Tubules

Crude lysates from ~125 female Malpighian tubules were prepared as described in a previous study (61). In brief, the tubules were homogenized in a high-urea buffer (51, 61, 80) and then an appropriate volume of a 5× Laemmli sample buffer (38) was added. Preliminary experiments indicated that our ability to detect *AeKCC1* immunoreactivity in tubule lysates was compromised when the samples were boiled. A similar phenomenon was observed by Su et al. (74) for mouse KCC1, which apparently forms SDS-resistant oligomers when incubated at temperatures $> 37^\circ\text{C}$. Thus, the crude tubule lysates in the present study were not boiled before loading onto polyacrylamide gels.

Proteins from the crude tubule lysates were 1) separated by molecular mass on a denaturing 8%-polyacrylamide gel and 2) transferred to an immunoblot PVDF membrane (Bio-Rad, Hercules, CA) as described previously (61, 62). The PVDF was washed with Tween-Tris-buffered saline (TTBS; 10 mM Tris-HCl, 150 mM NaCl, 0.01% Tween-20, pH 7.4) and blocked with 5% nonfat dry milk dissolved in TTBS (blocking buffer), as described previously (61, 62). The blocked PVDF membrane was incubated for 1 h with the anti-*AeKCC1* antibody (3.6 $\mu\text{g}/\text{ml}$ in blocking buffer) or the anti-*AeKCC1-A* antibody preabsorbed with its immunogenic peptide in a 25:1 molar ratio (peptide/antibody). Immunoreactivity was detected with a horseradish peroxidase (HRP)-conjugated goat anti-rabbit secondary antibody (Pierce Biotechnology), an enhanced chemiluminescence kit (SuperSignal West Pico; Pierce Biotechnology), and X-ray film as described previously (61, 62).

Immunolabeling of Malpighian Tubules

To localize the expression of *AeKCC1* in sections of Malpighian tubules, ~150 tubules were fixed and processed for routine paraffin embedding as described in a previous study (62). Sections of the tubules (4 μm) were adhered to ProbeOn Plus glass slides (Fisher Scientific), deparaffinized, rehydrated, and peroxide/methanol treated as described previously (62).

After the above steps, the sections were submitted to a wet autoclave antigen retrieval treatment (2), which reduces the nonspecific labeling and/or increases the sensitivity of polyclonal antibodies on paraffin sections of mosquito tissues (unpublished observations). The sections were autoclaved (120°C; 20 psi) for 15 min in a plastic Coplin jar containing 0.01 M sodium citrate buffer (pH 6.0). Following autoclaving, the sections were allowed to cool in the citrate buffer for 15 min at room temperature before being washed with distilled

H_2O and PBS (Fisher Scientific) for 5 min each. The remaining steps were all conducted at room temperature unless noted otherwise.

After antigen retrieval, the sections were blocked for 20 min with a histo-blocking buffer consisting of 10% normal goat serum (Invitrogen) supplemented with a $\times 2$ solution of casein (Vector Laboratories, Burlingame, CA). The sections were then incubated overnight at 4°C in a humidified chamber with one of the following: 1) PBS supplemented with $\times 1$ casein (Vector Laboratories), 2) the anti-*AeKCC1* antibody (1.8 $\mu g/ml$ in PBS-casein), or 3) the anti-*AeKCC1* antibody preabsorbed with its immunogenic peptide in a 25-to-1 molar ratio (peptide/antibody).

On the following day, the sections were rinsed and washed with PBS and then incubated for 20 min with a biotinylated goat anti-rabbit secondary antibody (Vector Laboratories). To visualize the binding of the antibodies, the sections were 1) treated with streptavidin-HRP (Vector Laboratories) for 30 min, 2) rinsed/washed with PBS, and 3) incubated with a chromogenic substrate of HRP (ImmPACT AEC; Vector Laboratories) for 10 min. The sections were dipped in Harris's hematoxylin (Electron Microscopy Sciences, Hatfield, PA) to counterstain, and then covered with a coverglass for brightfield viewing on an AX70 compound microscope (Olympus, Melville, NY).

Assays of Transepithelial Fluid Secretion

Rates of transepithelial fluid secretion were measured in isolated Malpighian tubules following the method of Ramsay (65) and as detailed in a recent study (69). In brief, a single, isolated Malpighian tubule was transferred to a droplet of Ringer solution (50 μl) covered with light mineral oil (Fisher Scientific). The open proximal end of the tubule was pulled into the surrounding oil with a silanized glass hook, allowing the distal blind end to remain in the Ringer solution. The fluid secreted by the distal tubule exits the proximal end of the lumen into the oil as a spherical droplet. The volume secreted is calculated by measuring the diameter of the droplet with an ocular micrometer.

In the Ramsay method (65), each tubule serves as its own control. In some experiments, the spontaneous, unstimulated rates of fluid secretion were first determined (over 30 min), and DIOA was then added to the Ringer droplet (10 μM final concentration) to examine its effects on fluid secretion over the next 30 min. This low concentration of DIOA was chosen to avoid the potential off-target effects of DIOA on P-type ATPases and mitochondria (17, 63). In other experiments, after measuring the initial control unstimulated rates of fluid secretion, adeskinin III (AKIII) or dibutryl-cAMP (db-cAMP; Sigma) was added to the Ringer droplet (10 $^{-6}$ M or 10 $^{-3}$ M final concentration, respectively). After the ensuing diuretic rate of fluid secretion was measured for 30 min, DIOA was added to the Ringer droplet, and the resulting secretion rate was measured over the next 30 min. The AKIII was synthesized and generously provided by the laboratory of Zubrak et al. (88).

Note that in all DIOA experiments the vehicle (DMSO) was present at a final concentration of 0.05%. Preliminary experiments determined that this concentration of DMSO affects neither the control rates nor the diuretic rates of fluid secretion (data not shown).

Two-Electrode Voltage Clamping of Principal Cells

The basal-membrane potential (V_b) and input resistance (R_{pc}) of principal cells was measured in isolated Malpighian tubules using the two-electrode voltage clamping approach developed by our laboratory (44). In brief, an isolated Malpighian tubule was attached to a small sheet of parafilm (American National Can, Menasha, WI) stretched over the bottom of a perfusion bath filled with Ringer solution (500- μl capacity). A single principal cell near the distal end of the tubule was then impaled with two microelectrodes. The microelectrodes were fabricated from borosilicate glass (cat. no. 1B100F-4; World Precision Instruments, Sarasota, FL), which was pulled on a programmable puller (model P-97; Sutter Instruments, Novato, CA) to yield resistances between 10 and 40 M Ω when filled with 3 M KCl.

To record the V_b and R_{pc} , the two microelectrodes were bridged to a Geneclamp 500 voltage amplifier (Molecular Devices, Sunnyvale, CA). One electrode reported the V_b , while the other electrode reported the basal membrane current (I_b). The latter only reported I_b during the application of a computer-controlled voltage-stepping protocol (see below). The output of both microelectrodes was recorded digitally by a Digidata 1440A (Molecular Devices) and the Axoscope module of the pCLAMP software (Version 10; Molecular Devices).

The R_{pc} was determined from current-voltage (I - V) plots generated by voltage clamping a principal cell in a sequence of voltage steps. That is, the principal cell was held at a hyperpolarizing voltage of 10 mV relative to its spontaneous V_b (i.e., V_b , -10 mV) and subjected to five subsequent depolarizing voltage steps of 5 mV held for 400 ms each. The voltage-clamp protocol was implemented, and the resulting I - V data were acquired digitally by the Digidata 1440A, as commanded by the Clampex module of the pCLAMP software package (Molecular Devices).

In the typical experiment, after recording a stable V_b and R_{pc} , DIOA (10 μM) was added to the peritubular Ringer solution. V_b and R_{pc} were monitored every 2–3 min thereafter until the principal cell reached a new steady state (typically 5–10 min). After this period, AKIII or db-cAMP was added to the peritubular bath (10 $^{-6}$ M and 10 $^{-3}$ M, respectively), and V_b and R_{pc} were again monitored. Preliminary experiments showed that individual principal cells exhibited variable and inconsistent responses in V_b and R_{pc} to repeated exposures of AKIII or db-cAMP, some of which have been previously documented (69). Thus, instead of a paired experimental design where a principal cell serves as its own control, the effects of DIOA on the electrophysiological responses of a principal cell to AKIII or db-cAMP were evaluated by using an unpaired experimental design in which the responses of a principal cell treated with DIOA were compared with those of a principal cell from an independent control tubule treated with the vehicle for DIOA (0.005% DMSO).

Statistics

Statistical analyses were performed using Graphpad Prism 5 (Graphpad Software, San Diego, CA). Comparisons between two groups were evaluated with an unpaired or paired *t*-test. To compare means among more than two groups, a one-way or repeated-measures ANOVA was used. If needed, multiple comparisons were performed with a Newman-Keuls posttest.

RESULTS

Molecular Cloning of *AeKCC1* Transcripts from *Aedes* Malpighian Tubules

5'-RACE experiments. As illustrated in Fig. 1A, the 5'-RACE experiments uncovered five distinct, alternatively spliced, partial transcripts of *AeKCC1* that are expressed in Malpighian tubules. We designate these variants as *AeKCC1-A₁*, *-A₂*, *-B₁*, *-B₂*, and *-C*. The *AeKCC1-A₁* and *-A₂* variants differ in both the nucleotide sequence and length of their most upstream 5'-untranslated regions (see orange vs. green, respectively, in Fig. 1A). However, both are expected to encode identical *AeKCC1-A* polypeptides, as indicated by the common start of their respective ORFs (see respective yellow-highlighted vertical bars in Fig. 1A).

The *AeKCC1-B₁* variant closely resembles the *AeKCC1-A* transcripts, but contains a truncated 5'-untranslated region (UTR) and is missing 134 bp (see dashed line in Fig. 1A) in the predicted ORF. Significantly, the absence of these 134 bp shifts the start of the ORF toward the 3'-end of the transcript compared with those of the *AeKCC1-A* variants

(see respective positions of yellow-highlighted vertical bars in Fig. 1A), resulting in a unique, truncated NH₂-terminal polypeptide sequence (described below and in Fig. 6). Although AeKCC1-B₂ contains a novel 5'-UTR compared with AeKCC1-B₁ (see blue vs. gray, respectively, in Fig. 1A), both are expected to encode identical AeKCC1-B polypeptides (see respective positions of yellow-highlighted vertical bars in Fig. 1A).

Finally, Fig. 1A shows that the AeKCC1-C variant closely resembles AeKCC1-B₂, but contains the region of 134 bp (dark grey) that is absent from the AeKCC1-B variants. Significantly, the presence of this 134-bp region shifts the start of the ORF toward the 5'-end of the transcript relative to the AeKCC1-A and -B variants (see relative positions of the respective yellow-highlighted vertical bars in Fig. 1A), resulting in yet another unique NH₂-terminal polypeptide sequence (described below and in Fig. 6).

To estimate which of the above cDNAs (if any) is expressed most abundantly in Malpighian tubules, we resolved the identity of 112 randomly screened bacterial colonies containing 5'-RACE products. We estimate (in % of screened colonies) that AeKCC1-A₁ is the most abundant (79.5%), followed by AeKCC1-B₁ (14%), AeKCC1-C (4.5%), AeKCC1-A₂ (1%), and AeKCC1-B₂ (1%). Consistent with this estimate are results from qualitative RT-PCR experiments on Malpighian tubule cDNA using a pair of gene-specific primers that 1) bind to regions common to the AeKCC1-A variants and AeKCC1-B₁ and 2) flank the 134-bp region missing from AeKCC1-B₁. As shown in Fig. 1B, the primer pair amplifies a product of ~600 bp, which is close to that expected for the amplification of the AeKCC1-A₁ or A₂ transcripts (607 bp). A PCR product of the expected size for AeKCC1-B₁ (473 bp) is not detectable. Using a similar approach with a pair of gene-specific primers that bind to regions common to both AeKCC1-B₂ and AeKCC1-C, PCR products of the expected sizes for either transcript were not detectable (data not shown). Taken together, the above results indicate that AeKCC1-A₁ is the majority transcript expressed in Malpighian tubules.

3'-RACE experiments. In contrast to the diversity of transcripts revealed by the 5'-RACE, the 3'-RACE experiments revealed no evidence for alternative splicing of AeKCC1 transcripts in either the 3'-end of the ORF or the 3'-UTR. Thus, we presume that the compositions of the AeKCC1 transcripts downstream to the regions shown in Fig. 1A are identical.

Cloning of the full-length AeKCC1-A₁ cDNA. Given the apparent majority of the AeKCC1-A₁ transcript in Malpighian tubules, we focused our efforts on cloning its full-length cDNA. As illustrated in Fig. 1C, we assembled a 5,233-bp transcript (excluding a poly-adenosine tail of at least 23 bp) corresponding to AeKCC1-A₁. The cDNA consists of a 5'-UTR of 393 bp, an ORF of 3,288 bp, and a 3'-UTR of 1,552 bp (Fig. 1C). To our knowledge, AeKCC1-A₁ represents the first SLC12-like KCC to be cloned from any insect Malpighian tubule.

Structure of the AeKCC1 Gene

By mapping the sequences of the cloned 1) alternatively spliced, partial cDNAs (Fig. 1A) and 2) full-length AeKCC1-A₁ cDNA (Fig. 1C) onto the *Aedes* genomic scaffold

(52), we deciphered the structure of the AeKCC1 gene. In brief, the gene is enormous. As shown in Fig. 2A, the AeKCC1 gene consists of at least 26 exons (drawn to a fixed-length for clarity) separated by 25 introns (drawn to scale) that together span over 429 kb in supercontig 1.532 and 542 kb in supercontig 1.614, reaching nearly 1 Mb in total length. Figure 2B illustrates the length of each exon (to scale) with a fixed intron length. Table 3 lists the positions and lengths of the above exons and introns in the *Aedes* genome. Note that the extreme length of the gene is not due to the total number of exons, which is a similar number to that for the KCC genes of mammals (i.e., 24–26 exons) (1) and *Drosophila* (i.e., 23 exons) (28), but rather to the presence of exceedingly long introns. For example, note the ~500 kb intron between exons 4 and -5 and the ~150 kb intron between exons 6 and 7 (Fig. 2A, Table 3), each of which alone exceeds the length of any mammalian KCC gene. Such lengthy introns are notorious in *Aedes* genes and have been attributed to the accumulation of transposable elements within introns (52).

Finally, Fig. 2, C and D illustrates how each of the 26 exons in the AeKCC1 gene contributes to the structural features of the cloned cDNAs described in Fig. 1. As shown in Fig. 2C, the variability in the 5'-end of the transcripts is attributed to the arrangement of the first nine exons. Notably, the missing stretch of 134 bp that characterizes the AeKCC1-B variants corresponds to the excision of exon 9. Exons 10–26 are expected to be present in all of the transcripts as occurs in AeKCC1-A₁ (Fig. 2D), given the results of the 3'-RACE experiments (see above).

Proteins Encoded by the AeKCC1 Gene

The ORF of the AeKCC1-A₁ cDNA is predicted to encode 1,096 amino acids (121.4 kDa) that on average share 54% identity to the human SLC12 KCCs (SLC12A4-A7) and 24% identity to the human SLC12 Na⁺-coupled Cl⁻-cotransporters (SLC12A1–3). We designate the encoded protein simply as AeKCC1-A (no subscript), because we do not expect differences between the sequence of amino acids encoded by the AeKCC1-A₁ and AeKCC1-A₂ transcripts.

A neighbor-joining phylogenetic tree (Fig. 3) shows the relationship of the predicted AeKCC1-A protein to other SLC12 cation-coupled Cl⁻ cotransporters from *D. melanogaster* and humans. The branching pattern of the tree indicates that the AeKCC1-A protein 1) shares a common node with the KCC of *Drosophila* (*DrKCC1*) and 2) occurs within a larger branch of the tree that includes the human (*Ho*) KCCs (Fig. 3). Among the human KCCs, the insect KCCs (i.e., AeKCC1-A and *DrKCC1*) appear to be more closely related to the branch that includes *HoKCC1* and *HoKCC3*, relative to the branch that includes *HoKCC2* and *HoKCC4* (Fig. 3). On the other hand, the Na⁺-coupled Cl⁻ cotransporters of both insects and humans occur in their own branch of the tree that is separate from the KCCs (Fig. 3).

Fig. 4A shows a Kyte-Doolittle analysis of the predicted AeKCC1-A protein (blue trace), which reveals the general topological arrangement of SLC12-like proteins (1, 21, 26). Specifically, AeKCC1-A begins with a short, hydrophilic NH₂-terminal domain of ~100 residues, followed by a transmembrane domain of ~500 residues and ends with a long, hydrophilic COOH-terminal domain of ~500 residues (Fig. 4A).

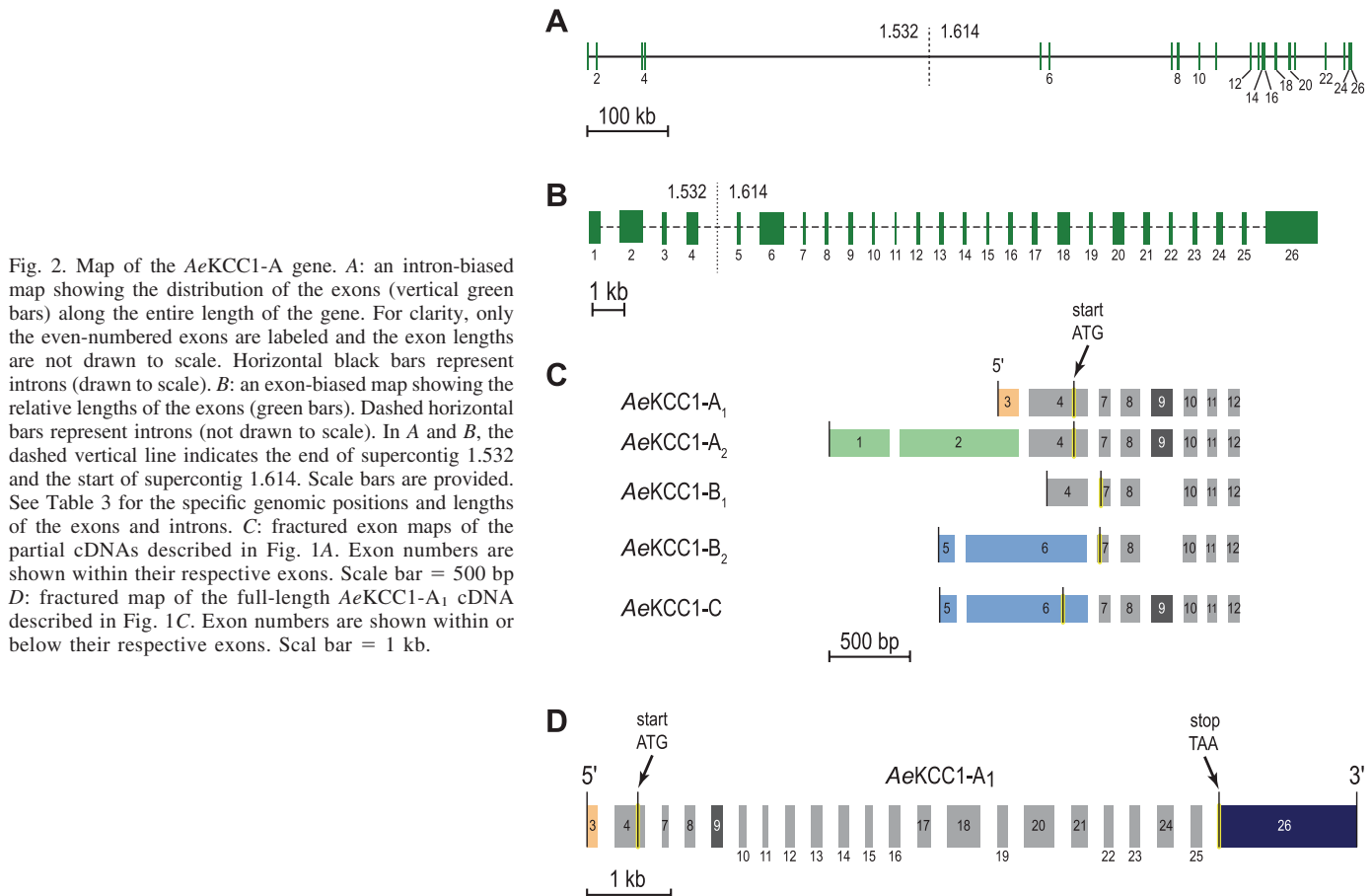


Fig. 2. Map of the AeKCC1-A gene. *A*: an intron-biased map showing the distribution of the exons (vertical green bars) along the entire length of the gene. For clarity, only the even-numbered exons are labeled and the exon lengths are not drawn to scale. Horizontal black bars represent introns (drawn to scale). *B*: an exon-biased map showing the relative lengths of the exons (green bars). Dashed horizontal bars represent introns (not drawn to scale). In *A* and *B*, the dashed vertical line indicates the end of supercontig 1.532 and the start of supercontig 1.614. Scale bars are provided. See Table 3 for the specific genomic positions and lengths of the exons and introns. *C*: fractured exon maps of the partial cDNAs described in Fig. 1A. Exon numbers are shown within their respective exons. Scale bar = 500 bp. *D*: fractured map of the full-length AeKCC1-A₁ cDNA described in Fig. 1C. Exon numbers are shown within or below their respective exons. Scale bar = 1 kb.

To assign predicted transmembrane segments within the transmembrane domain of AeKCC1-A, we aligned its hydrophyt plot with that of *HoKCC1* (red tracing in Fig. 4A). The transmembrane domains of AeKCC1-A and *HoKCC1* exhibit a very similar hydrophyt pattern (Fig. 4A), indicating that the proposed transmembrane assignments for mammalian KCCs (23, 31, 57) are applicable to AeKCC1-A. As such, we hypothesize that the transmembrane domain of AeKCC1-A consists of 12 hydrophobic transmembrane segments (gray bars in Fig. 4A) that are connected by relatively hydrophilic endofacial and exofacial loops, resulting in the putative topological model of AeKCC1-A (Fig. 4B). The amino acid residues that correspond to the predicted transmembrane segments are identified by the numbered horizontal bars in Fig. 5.

Predicted sites of posttranslational modification and regulation. Figure 5 presents the amino acid sequence of AeKCC1-A aligned with that of *Drosophila* KCC1-D and human KCC3-B. The red box near the NH₂-terminal domain of AeKCC1-A contains a predicted Ste20-related proline-alanine-rich kinase (SPAK)-binding motif (R/H-F-X-V), which is conserved in several SLC12 proteins (21, 60). In addition, as indicated by the open circles (Fig. 5) the NH₂-terminal domain contains several predicted sites of phosphorylation.

The transmembrane domain of AeKCC1-A contains two putative sites of N-glycosylation on the long exofacial loop connecting transmembrane segments 5 and 6 (i.e., the 5–6 loop; see also Fig. 4). Following the 5–6 loop, a few putative sites of phosphorylation occur on the endofacial 8–9 and 10–11 loops (○ in Fig. 5).

The long COOH-terminal domain of AeKCC1-A contains several putative sites of phosphorylation (○ in Fig. 5) and a threonine residue (Thr⁸⁸⁸) that is known to be phosphorylated in mammalian KCCs (● in Fig. 5) (66). Another important residue in the COOH-terminal domain of AeKCC1-A is Tyr¹⁰⁶⁷ (green Y in Fig. 5), which is a highly conserved tyrosine among all KCCs that plays a critical role in the functional expression of KCCs, possibly by modulating protein-protein interactions (73). Finally, conspicuous by its absence in the COOH-terminal domain of AeKCC1-A is the so-called isotonic domain of mammalian KCC2 isoforms, which confers constitutive activity to these isoforms under isotonic conditions when they are expressed in *Xenopus* oocytes (46). Thus, AeKCC1-A is expected to exhibit nominal transport activity under isotonic conditions when expressed in *Xenopus* oocytes.

Effects of alternative splicing on the composition of the NH₂-terminal domain. Fig. 6 illustrates the consequences of the alternative splicing that occurs in the 5' end of the AeKCC1 transcripts (Figs. 1A and 2C) on the amino acid sequence of the encoded proteins. The differences are primarily in the length and sequence of the extreme NH₂-terminal domain (see dashed box in Fig. 6), which contains several putative sites of phosphorylation and a putative SPAK-binding motif (Fig. 5). The downstream sequence of the remaining NH₂-terminal domain and the beginning of the transmembrane domain are identical in AeKCC1-A and AeKCC1-C (Fig. 6). In contrast, the comparable regions of the AeKCC1-B protein are substantially

Table 3. Positions and lengths of AeKCC1 exons and introns in the *Aedes* genome

Exon	Supercontig	Start Position	End Position	Length of Exon, bp	Length of Following Intron, bp
1	1.532	429,394	429,025	370	12,031
2	1.532	416,993	416,260	734	57,825
3	1.532	358,434	358,309	126	4,967
4	1.532	353,341	352,978	364	491,184*
5	1.614	585,831	585,730	102	12,468
6	1.614	573,261	572,513	749	153,537
7	1.614	418,975	418,905	71	8,062
8	1.614	410,842	410,722	121	763
9	1.614	409,958	409,825	133	27,442
10	1.614	382,382	382,300	83	21,910
11	1.614	360,389	360,287	61	44,448
12	1.614	315,838	315,733	106	10,485
13	1.614	305,247	305,118	130	6,706
14	1.614	298,411	298,290	122	96
15	1.614	298,193	298,111	83	1,364
16	1.614	296,746	296,611	136	13,744
17	1.614	282,866	282,710	157	620
18	1.614	282,089	281,695	395	17,552
19	1.614	264,142	264,025	118	596
20	1.614	263,428	263,066	363	6,931
21	1.614	256,134	255,945	190	39,716
22	1.614	216,228	216,121	108	25,079
23	1.614	191,041	190,913	129	6,693
24	1.614	184,219	184,023	197	225
25	1.614	183,797	183,658	140	575
26	1.614	183,082	181,441	1,642	n/a

*Assumes supercontig 1.614 is sequential to supercontig 1.532.

truncated (Fig. 6). The potential significance of the above differences will be explained in DISCUSSION.

Functional Characterization of AeKCC1-A Expressed Heterologously in *Xenopus* Oocytes

To characterize the function of AeKCC1-A, we expressed it heterologously in *Xenopus* oocytes and measured the unidirectional uptake rates of $^{86}\text{Rb}^+$, as a tracer for K^+ transport. Oocytes injected with H_2O served as controls. A similar approach has been used to characterize the functional and pharmacological properties of heterologous and endogenous KCCs in *Xenopus* oocytes (29, 47, 48, 50, 74, 77).

Effects of NEM on AeKCC1-A mediated $^{86}\text{Rb}^+$ transport. The rate of $^{86}\text{Rb}^+$ uptake in AeKCC1-A oocytes is slow ($33.9 \pm 4.7 \text{ fmol}\cdot\text{oocyte}^{-1}\cdot\text{h}^{-1}$) when they are bathed in an isotonic solution (200 osmol/kg) containing Cl^- (55.7 mM) (+ Cl^- – NEM in Fig. 7A). Compared with this isotonic rate of $^{86}\text{Rb}^+$ uptake, the rate is modestly, but significantly, faster ($77.72 \pm 13.2 \text{ fmol}\cdot\text{oocyte}^{-1}\cdot\text{h}^{-1}$) in AeKCC1-A oocytes that are bathed in the same isotonic solution containing 1 mM of the alkylating agent NEM (+ Cl^- + NEM in Fig. 7A). However, if AeKCC1-A oocytes are bathed in an isotonic solution containing a low concentration of Cl^- (0.07 mM) and NEM (– Cl^- + NEM in Fig. 7A), then the rate of $^{86}\text{Rb}^+$ uptake ($27.0 \pm 12.4 \text{ fmol}\cdot\text{oocyte}^{-1}\cdot\text{h}^{-1}$) is statistically similar to the isotonic rate. These results evince an NEM-stimulated, Cl^- -dependent uptake of $^{86}\text{Rb}^+$ in AeKCC1-A oocytes. In H_2O -injected oocytes, the rate of $^{86}\text{Rb}^+$ uptake is not significantly affected by the presence of NEM in the isotonic bath solution, regardless of the concentration of extracellular Cl^- (Fig. 7A).

Effects of external osmolality and Cl^- on AeKCC1-A-mediated $^{86}\text{Rb}^+$ transport. As was shown in Fig. 7A, the isotonic rate of $^{86}\text{Rb}^+$ uptake in AeKCC1-A oocytes is slow ($57.2 \pm 20.2 \text{ fmol}\cdot\text{oocyte}^{-1}\cdot\text{h}^{-1}$) (Iso + Cl^- in Fig. 7B). Compared with this slow isotonic rate of $^{86}\text{Rb}^+$ uptake, the rate is dramatically and significantly faster ($1,185 \pm 132.5 \text{ fmol}\cdot\text{oocyte}^{-1}\cdot\text{h}^{-1}$) in AeKCC1-A oocytes that are bathed in a hypotonic solution (100 osmol/kg) containing Cl^- (Hypo + Cl^- in Fig. 7B). However, if the AeKCC1-A oocytes are bathed in a hypotonic solution containing a low concentration of Cl^- (Hypo – Cl^- in Fig. 7B), then the rate of $^{86}\text{Rb}^+$ uptake ($53.6 \pm 22.9 \text{ fmol}\cdot\text{oocyte}^{-1}\cdot\text{h}^{-1}$) is statistically similar to the isotonic rate (Fig. 7B). These results are indicative of a Cl^- -dependent uptake of Rb^+ in AeKCC1-A oocytes that is activated profoundly by cell swelling.

In H_2O -injected oocytes, the rate of $^{86}\text{Rb}^+$ uptake is also significantly elevated, relative to the respective isotonic rate, when the oocytes are bathed in a hypotonic solution containing Cl^- (Fig. 7B). However, the hypotonic rate of H_2O -injected oocytes ($159 \pm 42.3 \text{ fmol}\cdot\text{oocyte}^{-1}\cdot\text{h}^{-1}$) is far less than that measured in the AeKCC1-A oocytes (see above) and is not affected by lowering the concentration of Cl^- (Fig. 7B).

Effects of DIOA and loop diuretics on AeKCC1-A mediated $^{86}\text{Rb}^+$ transport. We next sought to determine whether the hypotonic rate of $^{86}\text{Rb}^+$ uptake in AeKCC1-A oocytes is sensitive to DIOA. As was observed in Fig. 7, the rate of $^{86}\text{Rb}^+$ uptake in AeKCC1-A oocytes is low ($33.7 \pm 11.9 \text{ fmol}\cdot\text{oocyte}^{-1}\cdot\text{h}^{-1}$) when they are bathed in an isotonic solution containing Cl^- (Iso – DIOA in Fig. 8A). Moreover, as

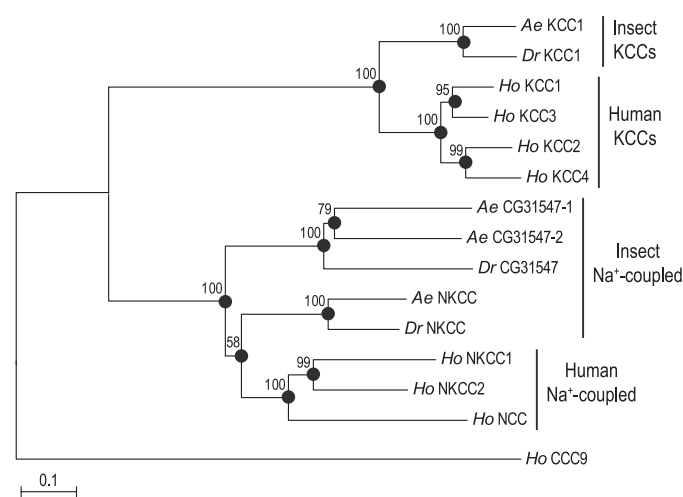


Fig. 3. Relationship of AeKCC1 to other cation-coupled chloride cotransporters. A neighbor-joining phylogenetic tree (using Poisson-corrected distance estimates) of amino acid sequences from select insect (*Ae*, *Aedes*; *Dr*, *Drosophila melanogaster*) and human (*Ho*, *Homo sapiens*) SLC12 proteins. Bootstrap scores (from 1,000 replicates) are provided for the nodes of the branches (●). The total branch length between 2 proteins represents the proportion of amino acids that differ between them. The scale bar corresponds to a proportional difference (branch length) of 0.1 (i.e., a 10% difference in amino acids). The tree is rooted to Human CCC9 (*HoCCC9*, *SLC12A8*), and was generated with MEGA 4 software (76). Accession nos. are *AeKCC1*, HM125960; *AeCG31547-1*, XP_001654082; *AeCG31547-2*, XP_001654083; *AeNKCC*, XP_001651829; *DrKCC1*, NP_726377; *DrCG31547*, NP_730938; *DrNKCC*, NP_648572; *HoKCC1*, NP_005063; *HoKCC2*, NP_001128243; *HoKCC3*, NP_005126; *HoKCC4*, NP_006589; *HoNCC*, EAW82888; *HoNKCC1*, AAB07364; *HoNKCC2*, NP_001037; *HoCCC9*, EAW79400.

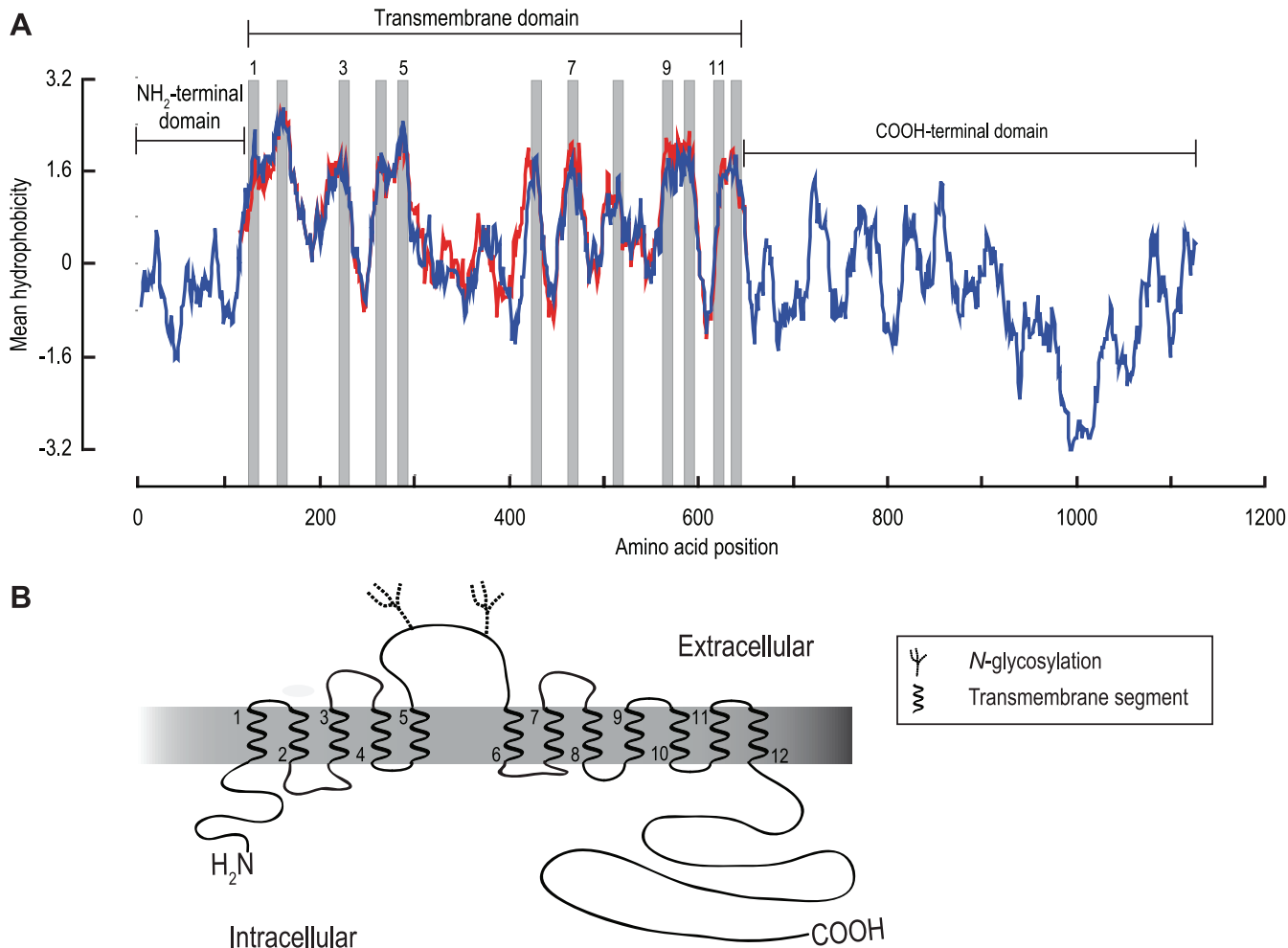


Fig. 4. Predicted membrane topology of the AeKCC1-A protein. *A:* plots of hydrophobicity (using a Kyte-Doolittle algorithm; window size = 19) for AeKCC1-A (blue) and the transmembrane domain of human KCC1 (red). The gray regions represent putative transmembrane segments following the assignments of previous investigators (23, 57). The plots were generated with the BioEdit Sequence Alignment Editor software, Version 7 (25). For clarity, only the odd-numbered transmembrane segments are labeled. Accession numbers are as follows: AeKCC1, HM125960; Human KCC1, NP_005063. *B:* hypothesized topology of AeKCC1-A based on the hydropathy plot in *A* and the topology model proposed for mammalian KCCs (26). Transmembrane segments are numbered at their emerging ends. Putative sites of *N*-glycosylation are indicated (see text and Fig. 5 for details).

was shown in Fig. 7A, relative to this isotonic rate of $^{86}\text{Rb}^+$ uptake, the rate is dramatically and significantly faster ($1,252 \pm 172.4$ fmol·oocyte $^{-1} \cdot \text{h}^{-1}$) in AeKCC1-A oocytes that are bathed in a hypotonic solution that contains Cl⁻ (Hypo – DIOA in Fig. 8A). However, if the AeKCC1-A oocytes are bathed in a hypotonic solution containing Cl⁻ and 100 μM DIOA (Hypo + DIOA in Fig. 8A), then their hypotonic rate of $^{86}\text{Rb}^+$ uptake is significantly dampened by 67% (416 ± 100.8 fmol·oocyte $^{-1} \cdot \text{h}^{-1}$).

As was observed in Fig. 7B, the hypotonic rate of $^{86}\text{Rb}^+$ uptake in H₂O-injected oocytes is significantly faster than the respective isotonic rate (Fig. 8A). However, the hypotonic rate of H₂O-injected oocytes (137.3 ± 57.3 fmol·oocyte $^{-1} \cdot \text{h}^{-1}$) is again far less than that observed in the AeKCC1-A oocytes (see above). Although the concentration of extracellular Cl⁻ did not affect the hypotonic rate of $^{86}\text{Rb}^+$ uptake in H₂O-injected oocytes (Fig. 7A), the presence of DIOA inhibits the hypotonic rate significantly by 71.5% (39.1 ± 12.65 fmol·oocyte $^{-1} \cdot \text{h}^{-1}$) (Fig. 8A).

Next, in AeKCC1-A oocytes, we compared the inhibitory effect of DIOA on the hypotonic rate of $^{86}\text{Rb}^+$ uptake with that

of other known inhibitors of SLC12 transporters. Figure 8B indicates that relative to the hypotonic rates of $^{86}\text{Rb}^+$ uptake in control AeKCC1-A oocytes, DIOA exhibits the most pronounced inhibition of $^{86}\text{Rb}^+$ uptake (67%), followed by furosemide (48%) and bumetanide (40%). The percent inhibitions elicited by the latter two loop diuretics are statistically similar to one another (Fig. 8B).

Role of *N*-Glycosylation in the Functional Expression of AeKCC1-A in Xenopus Oocytes

The above functional characterization experiments were conducted prior to the availability of the anti-AeKCC1 antibody. Thus, to validate the expression of an AeKCC1-A protein of the expected size in *Xenopus* oocytes, we used a tagged construct that fused eGFP to the COOH-terminal end of AeKCC1-A (i.e., AeKCC1-A-eGFP). As shown in Fig. 9A, Western blot analysis of membrane fractions isolated from AeKCC1-A-eGFP oocytes reveals two bands of GFP immunoreactivity at ~ 160 kDa and ~ 210 kDa, which are not present in membrane fractions isolated from H₂O-injected oocytes.

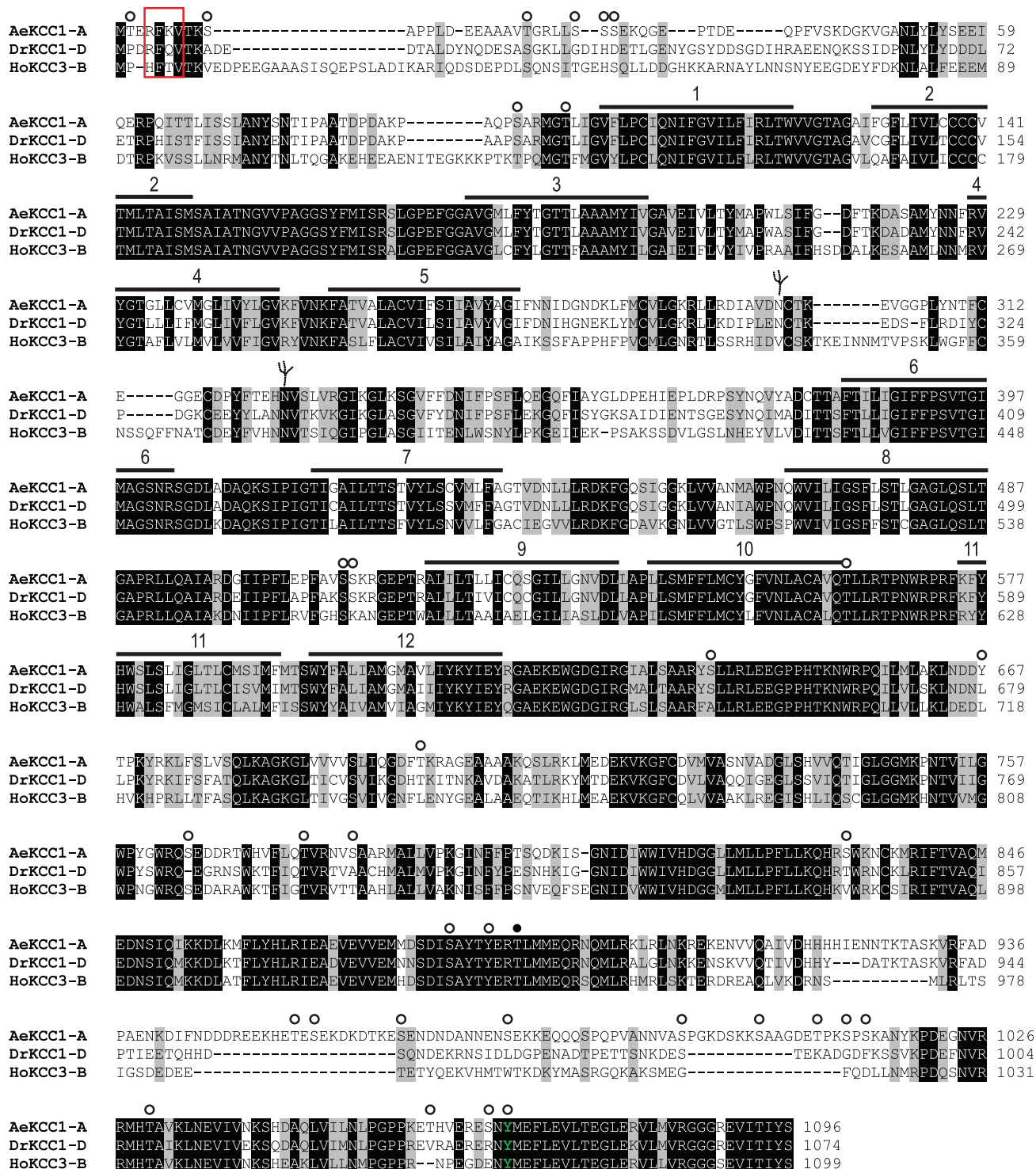


Fig. 5. Amino acid sequence of AeKCC1-A. The amino acids of AeKCC1-A (accession no. HM125960) are aligned with those of a *Drosophila* KCC isoform (*DrKCC1-D*; accession no. NP_726377) and a human KCC3 isoform (*HoKCC3-B*; accession no. NP_005126). The alignment was conducted with a ClustalW algorithm (39). The residue shading was performed with BioEdit Sequence Alignment software, Version 7 (25) using a threshold of 100%, where black shading indicates identical residues and gray shading indicates similar residues. Predicted transmembrane segments are indicated by the numbered horizontal bars. The red box near the NH₂-terminal end outlines a conserved Ste20-related proline-alanine-rich kinase (SPAK)-binding motif R/H F X V (21, 60). Circles indicate putative sites of phosphorylation (○) as predicted by a NetPhos 2.0 analysis (8) and (●) the known site of phosphorylation in mammalian KCCs that is conserved in AeKCC1-A and *DrKCC1-D* (66). The green tyrosine residue (Y1067 in AeKCC1-A) is known to play an important role in the functional expression of mammalian KCCs (73). Putative sites of N-linked glycosylation as predicted by a PROSCAN analysis (14) are labeled as in Fig. 4.

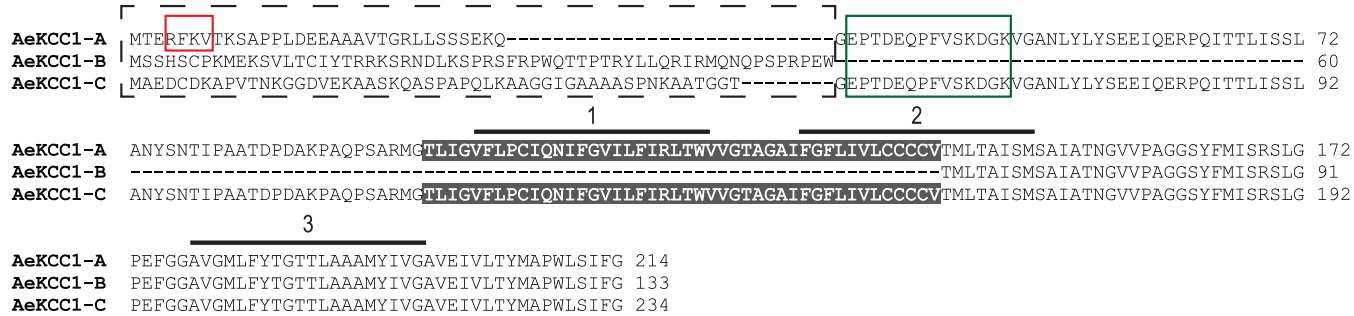


Fig. 6. Effects of splice variation on the amino acid sequence of *AeKCC1* proteins. The NH₂-terminal amino acids of *AeKCC1*-A (accession no. HM125960) are aligned with those of *AeKCC1*-B (accession no. JF958165) and *AeKCC1*-C (accession no. JF958168). The black dashed box indicates the novel components of the respective NH₂-terminal domains. Predicted transmembrane segments are indicated by the numbered horizontal bars. The red box near the NH₂ terminus outlines a conserved SPAK-binding motif R/H F X V, which is only found in *AeKCC1*-A. The green box outlines the region that corresponds to a synthetic peptide used to generate an anti-*AeKCC1* antibody. The dark gray region indicates the amino acids that are encoded by exon 9, which are missing in *AeKCC1*-B (see Fig. 2C). Note that this excision disrupts the first 2 predicted transmembrane segments.

Both of these bands are larger than the expected size of the *AeKCC1*-A-eGFP fusion protein (~150 kDa).

To determine whether the larger than expected sizes of the two bands are due to glycosylation of the *AeKCC1*-A-eGFP

fusion protein, we injected *Xenopus* oocytes with tunicamycin (an inhibitor of N-linked glycosylation) or DMSO (the tunicamycin vehicle) before injecting them with *AeKCC1*-A-eGFP cRNA. Whereas the injection of DMSO still results in the two immunoreactive bands, the injection of tunicamycin results in only a single band that exhibits a slightly greater mobility on SDS-PAGE compared with the 160 kDa form (Fig. 9B). Thus, an active biochemical pathway of N-linked glycosylation is

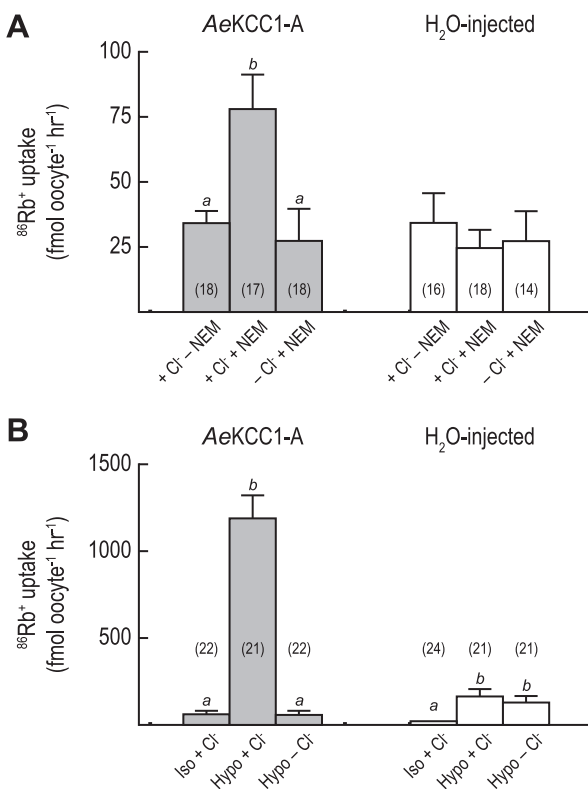


Fig. 7. Effects of N-ethylmaleimide (NEM), cell swelling, and extracellular Cl⁻ on the uptake of ⁸⁶Rb⁺ in *Xenopus* oocytes heterologously expressing *AeKCC1*-A. Both panels show the rates of ⁸⁶Rb⁺ uptake measured in *Xenopus* oocytes 5–7 days after injection with *AeKCC1*-A cRNA (28 ng) or H₂O (28 nl). Shaded bars represent rates of ⁸⁶Rb⁺ uptake in *AeKCC1*-A oocytes, whereas the white bars represent the corresponding rates in H₂O-injected oocytes. Values are means \pm SE, based on the number of oocytes in parentheses. Italicized letters indicate categorization of the means as determined by a one-way ANOVA and Newman-Keuls posttest ($P < 0.05$). Experimental conditions are indicated below the bars. A: + Cl⁻, 55.7 mM extracellular Cl⁻; - Cl⁻, 0.07 mM extracellular Cl⁻; and + NEM, 1 mM extracellular NEM. All solutions in A are isotonic (200 osmol/kg). B: Iso, isotonic solution of 200 osmol/kg; Hypo, hypotonic solution of 100 osmol/kg.

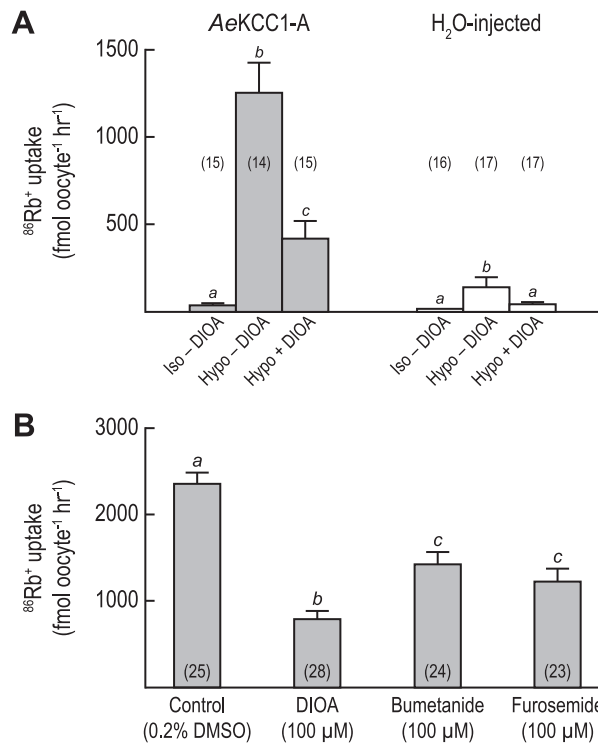


Fig. 8. Pharmacology of the uptake of ⁸⁶Rb⁺ in *Xenopus* oocytes heterologously expressing *AeKCC1*-A. A: rates of ⁸⁶Rb⁺ uptake measured in *Xenopus* oocytes 5–7 days after injection with *AeKCC1*-A cRNA (28 ng) or H₂O (28 nl). Bar shading, values, and italicized letters are as in Fig. 7. Experimental conditions are indicated below the bars. Iso and Hypo are as in Fig. 7; + DIOA indicates the presence of 100 μ M dihydroindenoxyalkanoic acid. All solutions contain 55.7 mM Cl⁻. B: shaded bars represent the hypotonic rates of ⁸⁶Rb⁺ uptake in *AeKCC1*-A oocytes (after subtraction of the isotonic rate) in the presence of external DMSO (the vehicle), DIOA, or a loop diuretic (bumetanide, furosemide). Values and italicized letters are as in Fig. 7.

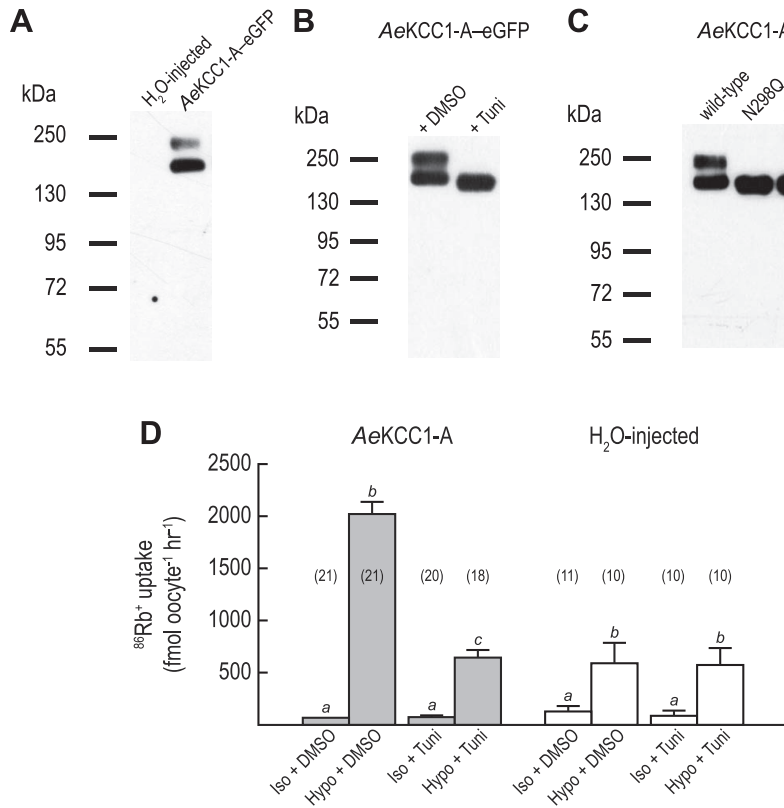


Fig. 9. Glycosylation of AeKCC1-A expressed heterologously in *Xenopus* oocytes. *A*: Western blot of total membrane fractions isolated from *Xenopus* oocytes 6 days after injection with H₂O (28 nl) or AeKCC1-A-eGFP cRNA (28 ng). A monoclonal anti-GFP antibody (JL-8) was used. Migrations of the molecular mass markers (in kDa) are left. *B*: Western blot of total membrane fractions isolated from AeKCC1-A-eGFP oocytes that were preinjected with DMSO or tunicamycin (Tuni). A monoclonal anti-GFP antibody (JL-8) was used. Migrations of the molecular mass markers (in kDa) are left. *C*: Western blot of total membrane fractions isolated from *Xenopus* oocytes injected with cRNA encoding AeKCC1-A-eGFP (wild-type) or a mutated AeKCC1-A-eGFP (N298Q, N325Q, or N298Q-N325Q). A monoclonal anti-GFP antibody (JL-8) was used. Migrations of the molecular mass markers (in kDa) are indicated to the left. *D*: rates of ⁸⁶Rb⁺ uptake measured in *Xenopus* oocytes 5–7 days after injection with AeKCC1-A cRNA (28 ng) or H₂O (28 nl). Bar shading, values, and italicized letters are as in Fig. 7. Experimental conditions are indicated below the bars. Iso and Hypo are as in Fig. 7; DMSO, preinjection of the oocytes with DMSO; + Tuni, preinjection with tunicamycin. All solutions contain 55.7 mM Cl⁻.

necessary for producing both the 160-kDa and 210-kDa forms of AeKCC1-A-eGFP in *Xenopus* oocytes.

As shown in Figs. 4 and 5, the 5–6 loop of AeKCC1-A contains two predicted sites of *N*-glycosylation: Asn²⁹⁸ and Asn³²⁵. To determine whether these sites are associated with the above *N*-glycosylation of AeKCC1-A, we examined the immunoreactivities of AeKCC1-A-eGFP fusion proteins containing mutations of the above asparagines (N) to glutamines (Q): two are single mutants (N298Q and N325Q) and one is a double mutant (N298Q-N325Q). Each of the mutant proteins is characterized by a single band of immunoreactivity that exhibits a slightly greater mobility on SDS-PAGE relative to the 160 kDa form in the wild-type AeKCC1-A-eGFP oocytes (Fig. 9C). Thus, Asn²⁹⁸ and Asn³²⁵ are both required to produce the 160 kDa and 210 kDa forms of AeKCC1-A.

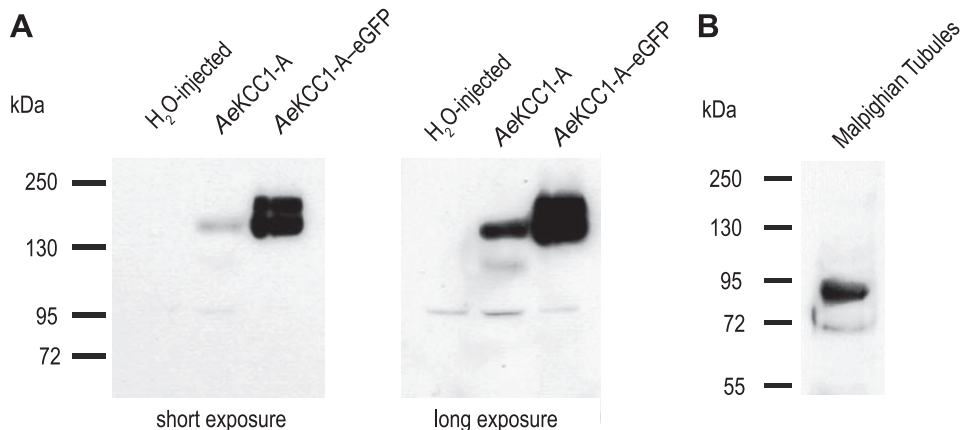
Finally, to determine whether *N*-glycosylation of AeKCC1-A is important for its functional expression in *Xenopus* oocytes, we conducted ⁸⁶Rb⁺ influx experiments on AeKCC1-A oocytes (and H₂O-injected oocytes) that were preinjected with either DMSO or tunicamycin. AeKCC1-A oocytes injected with DMSO exhibit the typical slow isotonic and fast hypotonic rates of ⁸⁶Rb⁺ uptake (Fig. 9D). In AeKCC1-A oocytes that are injected with tunicamycin, the isotonic rate of ⁸⁶Rb⁺ uptake is similar to that of the DMSO-injected oocytes, but the hypotonic rate is significantly dampened by 68% compared with that of the DMSO-injected oocytes (Fig. 9D). In the H₂O-injected oocytes, the preinjection of tunicamycin affects neither the isotonic nor the hypotonic rates of ⁸⁶Rb⁺ uptake, compared with those preinjected with DMSO (Fig. 9D). The above data indicate that *N*-glycosylation is important for the functional expression of AeKCC1-A in *Xenopus* oocytes.

Expression and Localization AeKCC1 Immunoreactivity in *Aedes* Malpighian Tubules

Validation of anti-AeKCC1 antibody. To test the effectiveness of the affinity-purified anti-AeKCC1 antibody, we first performed Western blot analysis on total membrane fractions isolated from *Xenopus* oocytes injected with H₂O, AeKCC1-A cRNA, or AeKCC1-A-eGFP cRNA. As shown in the short exposure of Fig. 10A, the anti-AeKCC1-A antibody primarily detects a weak band of protein at ~160 kDa in the AeKCC1-A oocytes that is not present in the H₂O-injected oocytes. In the long exposure of Fig. 10A, the 160-kDa band is more prominent, and a weak, diffuse band of ~120 kDa is revealed. This finding is consistent with our observations in Fig. 9 that AeKCC1-A is expressed in *Xenopus* oocytes as two differentially glycosylated forms. Importantly, in the AeKCC1-A-eGFP oocytes, the anti-AeKCC1 antibody detects the same two bands of protein at ~210 kDa and ~160 kDa (Fig. 10A) as the anti-GFP antibody (Fig. 9A).

Next, we performed Western blot analysis on crude lysates of adult female *Aedes* Malpighian tubules. As shown in Fig. 10B, the anti-AeKCC1-A antibody primarily detects a strong immunoreactive band of protein in Malpighian tubules around 87 kDa and a weaker band around 72 kDa. The presence of two immunoreactive bands is consistent with the expression of differentially glycosylated forms of AeKCC1 in Malpighian tubules, as we observe in *Xenopus* oocytes (Fig. 9, Fig. 10A). Although neither band matches the expected size of ~120 kDa for AeKCC1-A, the detection of each band is blocked when the anti-AeKCC1 antibody is

Fig. 10. Characterization of anti-AeKCC1 antibody. A: representative Western blots of total membrane fractions isolated from *Xenopus* oocytes 6 days after injection with H₂O, AeKCC1-A cRNA (28 ng), or AeKCC1-A-eGFP cRNA (28 ng). An anti-AeKCC1 antibody was used. Migrations of the molecular mass markers (in kDa) are left. A relatively short (10 s) or long (30 s) exposure of the X-ray film to the PVDF membrane is indicated. B: representative Western blot of crude lysates from Malpighian tubules of adult *Aedes* females. An anti-AeKCC1 antibody was used. Migrations of the molecular mass markers (in kDa) are indicated left.



preabsorbed with its immunogenic peptide (data not shown). Thus, the native AeKCC1 protein in Malpighian tubules likely runs anomalously of its size on SDS-PAGE, as we have observed previously for AeNHE8 and AeAE from Malpighian tubules (61, 62).

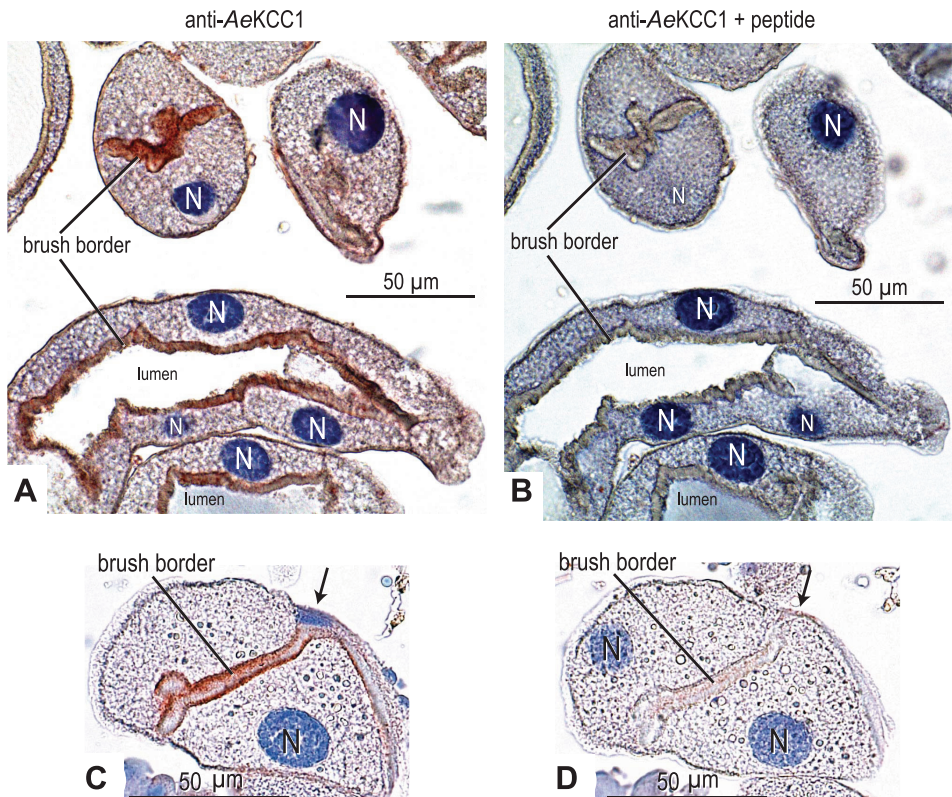
Localization of AeKCC1 immunoreactivity in *Aedes* Malpighian tubules. In sections of paraffin-embedded Malpighian tubules isolated from adult female mosquitoes, AeKCC1 immunoreactivity (red staining) occurs in the luminal brush border of principal cells (Fig. 11, A and C). Moreover, the immunolabeling of the brush border is blocked if the anti-AeKCC1 antibody is preabsorbed with its immunogenic peptide (Fig. 11, B and D). No immunolabeling is detected in stellate cells (e.g., arrow in Fig. 11C).

Effects of DIOA on Transepithelial Fluid Secretion in *Aedes* Malpighian Tubules

In the following experiments, we aimed to determine whether DIOA affects the rates of transepithelial fluid secretion mediated by isolated Malpighian tubules. As shown in Fig. 12A, Malpighian tubules secrete fluid at a mean rate of 0.46 ± 0.07 nl/min under control (unstimulated) conditions. The addition of DIOA to the Ringer bath (10 μ M) significantly inhibits the unstimulated rates of fluid secretion by $\sim 60\%$ to 0.19 ± 0.05 nl/min (Fig. 12A).

We next examined the effects of DIOA on tubules stimulated with the diuretic peptide AKIII, which employs Ca^{2+} as the second messenger to enhance transepithelial fluid secretion

Fig. 11. Immunoperoxidase localization of AeKCC1 in sections of Malpighian tubules. Representative immunolabeling of AeKCC1 in sections of paraffin-embedded Malpighian tubules isolated from adult *Aedes* females. The sections in A and B (and in C and D) are from the same Malpighian tubule taken 4 μ m apart. The red staining in A and C represents labeling by the anti-AeKCC1 antibody. In B and D, the antibody is preabsorbed with the immunogenic peptide. Sections are counterstained with hematoxylin to stain nuclei and provide contrast. N, nucleus of a principal cell; arrow in C and D, location of a stellate cell. Scale bars = 50 μ m.



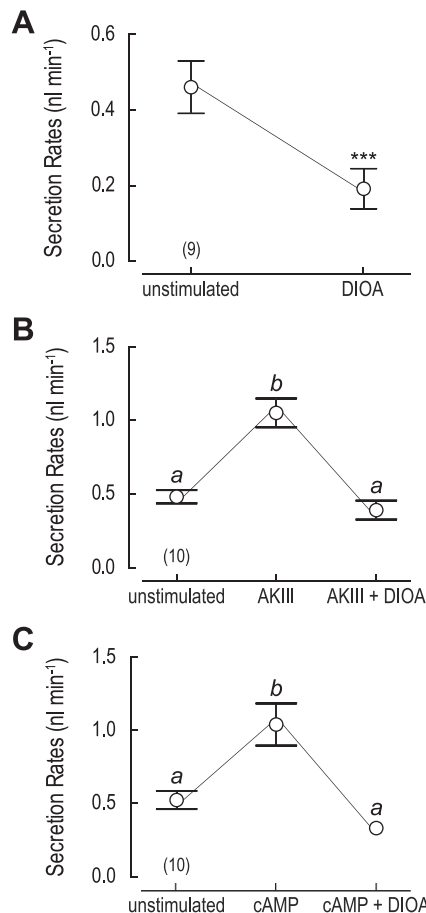


Fig. 12. Effects of DIOA on fluid-secretion rates of isolated *Aedes* Malpighian tubules. **A:** effect of 10 μM DIOA in control (unstimulated) Malpighian tubules. Transepithelial fluid secretion rates were measured in the absence (unstimulated) and presence of DIOA for 30 min, each in the same tubules. Open circles indicate secretion rates in means \pm SE for 9 Malpighian tubules. ***Significant difference ($P < 0.001$) as determined by a paired *t*-test. **B:** effect of 10 μM DIOA on the diuresis stimulated by AKIII (10^{-6} M). Each of 10 Malpighian tubules was first studied for 30 min under unstimulated conditions, then in the presence of AKIII, and finally in the presence of AKIII and DIOA. **C:** effect of 10 μM DIOA on the diuresis stimulated by db-cAMP (10^{-3} M) in each of 10 Malpighian tubules studied following the experimental protocol described in **B**. Italicized letters in **B** and **C** indicate categorization of the means as determined by a repeated-measures ANOVA and Newman-Keuls posttest ($P < 0.05$). For clarity, error bars are not drawn if smaller than the symbol.

(86). As shown in Fig. 12B, adding AKIII to the peritubular Ringer bath (10^{-6} M) significantly increases the mean fluid secretion rate over twofold from 0.49 ± 0.045 nl/min during the unstimulated period to 1.06 ± 0.10 nl/min. The subsequent addition of DIOA to the Ringer bath (10 μM) significantly reduces the mean fluid secretion rate by ~62% to 0.40 ± 0.06 nl/min (Fig. 12B).

DIOA has a similar effect on the diuretic rates of fluid secretion that are stimulated by db-cAMP, which is a membrane-permeable analog of the second message of the calcitonin-like diuretic peptide (13). As shown in Fig. 12C, adding db-cAMP (10^{-3} M) to the peritubular Ringer bath significantly increases the mean fluid secretion rate twofold from 0.52 ± 0.06 nl/min during the unstimulated period to 1.04 ± 0.14 nl/min (cAMP in Fig. 12C). The subsequent addition of DIOA

Table 4. Effects of DIOA (10 μM) on the electrophysiology of principal cells from unstimulated Malpighian tubules

Treatment	ΔV_b , mV	ΔR_{pc} , k Ω
DIOA, n = 24	+4.35 \pm 1.6	+22.1 \pm 7.4
DMSO, n = 18	+4.0 \pm 2.2	+20.6 \pm 11.1

Values are means \pm SE, based on the number of unpaired measurements indicated. V_b , basal-membrane potential; R_{pc} , input resistance; DIOA, dihydroindenoxyalkanoic acid. The DMSO group serves as a control.

to the Ringer bath significantly reduces the mean fluid secretion rate by ~68% to 0.33 ± 0.04 nl/min (Fig. 12C).

Effects of DIOA on the Electrophysiology of Principal Cells

To determine whether the above inhibitory effects of DIOA on transepithelial fluid secretion are associated with electrophysiological changes to the epithelium, we used the method of two-electrode voltage clamping in isolated *Aedes* Malpighian tubules to measure the basal membrane voltage (V_b) and input resistance (R_{pc}) of principal cells (44). As reported in Table 4, in unstimulated Malpighian tubules, the addition of DIOA to the peritubular bath modestly depolarizes the V_b and increases the R_{pc} of principal cells. However, statistically similar changes to the V_b and R_{pc} of principal cells are also observed in tubules treated with DMSO (Table 4), the vehicle for DIOA.

Next, we sought to determine whether DIOA prevents the known electrophysiological responses of principal cells to AKIII and db-cAMP (4, 69). As shown in Table 5, the AKIII-mediated hyperpolarization of V_b and drop in R_{pc} in principal cells is statistically similar between tubules treated with DIOA and those treated with DMSO (the vehicle for DIOA). Likewise, the db-cAMP-mediated depolarization of V_b and drop in R_{pc} in principal cells is statistically similar between tubules treated with DIOA and those treated with DMSO (Table 5). Since DIOA has no significant effect on tubule electrophysiology, but significantly reduces the transepithelial secretion of fluid in Malpighian tubules (Fig. 12), we conclude that DIOA inhibits an electroneutral transport mechanism, which is consistent with the blockage of a KCC (21).

DISCUSSION

AeKCC1 Gene Encodes Several Alternatively Spliced Transcripts

We have identified five alternatively spliced, partial cDNAs of the *AeKCC1* gene in *Aedes* Malpighian tubules that vary in the compositions and lengths of their 5'-ends (Fig. 1A). In some cases, the 5'-splicing of *AeKCC1* only influences the length and nucleotide composition of the 5'-UTR with no

Table 5. Effects of DIOA (10 μM) on the electrophysiology of principal cells from stimulated Malpighian tubules

Treatment	ΔV_b , mV	ΔR_{pc} , k Ω
DIOA + AKIII, n = 8	-16.9 \pm 3.6	-61.65 \pm 16.25
DMSO + AKIII, n = 9	-16.9 \pm 3.9	-80.8 \pm 16.6
DIOA + db-cAMP, n = 12	+47.9 \pm 4.85	-60.7 \pm 7.6
DMSO + db-cAMP, n = 10	+61.8 \pm 4.9	-83.5 \pm 12.0

Values are means \pm SE, based on the number of unpaired measurements indicated. AKIII, aedeskinin III; db-cAMP, dibutyl-cAMP. The DMSO group serves as a control.

apparent consequence on the encoded amino acids (i.e., *AeKCC1-A₁* vs. -*A₂* and *AeKCC1-B₁* vs. -*B₂*; Fig. 1A and Fig. 2C). The implications of such splicing in the 5'-UTR are unclear, but variations in the length and/or composition of the 5'-UTRs can affect the stability and secondary structure of mRNAs, as well as the accessibility of mRNAs to ribosomes, which together influence their translational efficiency (11, 59).

In other cases, the splicing results in a novel NH₂-terminal domain of the encoded *AeKCC1* protein. For example, the NH₂-terminal domain of the *AeKCC1-A* variant contains a putative SPAK-binding motif (21, 60) that is absent in the *AeKCC1-B* and *AeKCC1-C* variants (Fig. 6). Similar 5'-splicing phenomena regarding the presence or absence of an NH₂-terminal SPAK-binding motif are known to occur in mammalian KCC2 and KCC3, *Drosophila* KCC1, and *Caenorhabditis elegans* KCC2 (28, 49, 77, 79).

The functional significance of alternative splicing in the NH₂-terminal domain of any KCC is not well established. For example, SPAK appears to play only a minor role (if any) in regulating the transport activity of mammalian KCC isoforms-1, -3, and -4 (15, 22, 37, 66), with the exception of KCC2 (20). Moreover, variations in the amino acid sequence of the NH₂-terminal domain that arise from alternative splicing do not dramatically affect the K,Cl cotransport activity of mammalian KCC2 or KCC3 (49, 79). However, at least in the case of human KCC3, alternative splicing that changes the amino acid sequence of the NH₂-terminal domain can influence the ability of KCC3 to interact physically with the α -subunit of the Na⁺, K⁺-ATPase (16).

Among the *AeKCC1* splices we identified, the *AeKCC1-B* variants are exceptional in the excision of exon 9 (Figs. 1A and 2C). The excision is expected to 1) shorten the polypeptide by 44 amino acids (see dark gray region in Fig. 6), and 2) shift the start of the ORF toward the 3'-end of the transcript (Figs. 1A and 2C). Such a truncation of the NH₂-terminal domain may reduce the protein's functional activity (relative to *AeKCC1-A* and -C) given that the transport activity of human KCC1 is dampened by ~50% in engineered constructs missing the first 46 amino acids and is abolished altogether in engineered constructs missing the first 89 or 117 amino acids (10).

Among the 44 amino acids encoded by exon 9 are those associated with the first transmembrane segment and most of the second (see dark gray region in Fig. 6). Thus, the *AeKCC1-B* protein is expected to contain only 10 transmembrane domains in which transmembrane segment 3 of *AeKCC1-A* and *AeKCC1-C* would represent transmembrane segment 1 of *AeKCC1-B*. A similar splicing arrangement has been described by Mount et al. (50) who cloned a partial KCC4 cDNA from human skeletal muscle (via 5'-RACE) in which exon 4 is apparently excised; this exon encodes transmembrane segments 1 and 2 in KCC4 (50). The functional implications of insect or mammalian KCCs lacking the first two transmembrane segments remain to be determined, but it has been hypothesized that transmembrane segment 2 of mammalian KCCs serves as a site for the binding of K⁺ (56). Thus, if the KCC proteins encoded by the above transcripts have transport activity, then their functional properties may diverge significantly from those of the canonical KCCs (see below).

AeKCC1-A Protein Is a Canonical K,Cl Cotransporter

With few exceptions, the typical functional features of most KCCs are 1) a lack of transport activity in isotonic solutions, 2) an activation of K,Cl cotransport activity by exposure to alkylating agents (e.g., NEM) or to cell swelling, and 3) an inhibition of K,Cl cotransport activity by certain carboxylic acids (e.g., dihydroindenoxylalkanoic acid, DIOA) and the so-called loop diuretics (e.g., furosemide). *AeKCC1-A* exhibits all of these features when expressed heterologously in *Xenopus* oocytes.

Lack of isotonic activity. Figures 7 and 8A demonstrate that *AeKCC1-A* lacks the constitutive isotonic uptake of ⁸⁶Rb⁺ exhibited by mammalian KCC2 isoforms expressed in *Xenopus* oocytes (72, 73). Similar to *AeKCC1*, the only other insect KCC to be functionally characterized in *Xenopus* oocytes (i.e., *Drosophila* KCC1-B and -D) are inactive in isotonic solutions (29, 75). These findings are consistent with the observation that insect KCCs lack the so-called isotonic domain in their COOH-terminal domains, which has been shown to confer the constitutive isotonic activity of mammalian KCC2 isoforms expressed in *Xenopus* oocytes (46).

Activation by NEM and cell swelling. As shown in Fig. 7, both NEM and hypotonic cell swelling stimulate the rates of ⁸⁶Rb⁺ uptake in *AeKCC1-A* oocytes. Importantly, the uptake of extracellular ⁸⁶Rb⁺ requires the presence of extracellular Cl⁻, which is consistent with *AeKCC1-A* mediating K,Cl cotransport. NEM is thought to stimulate the transport activity of KCCs either directly via interactions with cysteine sulfhydryl groups or indirectly via the activation of phosphatases that dephosphorylate KCCs (40, 47), and cell swelling is thought to stimulate KCCs by signaling to the deactivation of kinases and the activation of phosphatases. Thus, alkylating agents and cell swelling activate KCCs via the dephosphorylation of KCCs (for recent reviews see Refs. 30, 37).

In *AeKCC1-A*, the degree of activation induced by cell swelling (~21-fold) is far greater than that induced by NEM (~2.3-fold) (Fig. 7), which is consistent with observations from previous characterizations of vertebrate KCCs in *Xenopus* oocytes (47, 48, 73, 74). The degree of activation by hypotonicity that we report for *AeKCC1-A* is also very similar to that observed by Hekmat-Scafe et al. (29) for *Drosophila* KCC1-B (~20-fold) expressed heterologously in *Xenopus* oocytes.

Inhibition by DIOA and loop diuretics. DIOA prominently dampens the hypotonic rate of ⁸⁶Rb⁺ uptake in *AeKCC1-A* oocytes (Fig. 8A). To our knowledge, this is the first direct evidence that DIOA blocks an insect KCC. This finding validates the efforts of other laboratories that have used DIOA as a pharmacological tool to inhibit KCC activity in insect Malpighian tubules (24, 42). Moreover, DIOA is a significantly more effective inhibitor of the hypotonic *AeKCC1-A* activity than bumetanide and furosemide (Fig. 8B). Previous studies on the endogenous *Xenopus* oocyte KCC and human KCC4 (expressed in *Xenopus* oocytes) have also observed that DIOA is a more effective inhibitor of hypotonic KCC transport than bumetanide and furosemide. In contrast, human KCC1 (expressed in *Xenopus* oocytes) is less sensitive to DIOA than to bumetanide and furosemide (48).

AeKCC1-A Protein Requires N-Glycosylation for Its Functional Expression

To our knowledge, sites of *N*-glycosylation in the extracellular 5–6 loop of KCCs have been predicted in every full-length KCC cDNA that has been cloned from the first mammalian KCCs (23, 57) to the present mosquito KCC (Figs. 4 and 5). Moreover, biochemical experiments on mammalian KCCs expressed heterologously and in native tissues have demonstrated that KCCs are indeed *N*-glycosylated (e.g., 23, 56, 74). Our present study provides the first direct evidence that the 5–6 loop of KCCs is glycosylated and that this glycosylation is important for their functional expression (discussed below).

Evidence for, and the sites of, N-glycosylation. Our Western blot analysis experiments in *Xenopus* oocytes with the AeKCC1-A-eGFP construct indicate that AeKCC1-A is *N*-glycosylated, as evidenced by its expression as two larger-than-expected forms (~210 kDa and ~160 kDa) in the absence of tunicamycin (Fig. 9, A and B) and one form of the expected size (~150 kDa) in the presence of tunicamycin (Fig. 9B). We presume that the ~210 kDa form represents a complex KCC glycoprotein, whereas the ~160 kDa form represents a high-mannose KCC glycoprotein, as reported for rat NCC and NKCC2 expressed in *Xenopus* oocytes (32, 55).

As shown in Fig. 9C, both Asn²⁹⁸ and Asn³²⁵ of the extracellular 5–6 loop are required to produce the complex and high-mannose AeKCC1-A glycoproteins, because the mutation of either site (or both sites) results in the expression of a single nonglycosylated form of the expected size. Our findings in AeKCC1-A are consistent with those from previous studies on rat NCC and NKCC2, which also have two extracellular, consensus sites of *N*-glycosylation that are required to produce the complex NCC and NKCC2 glycoproteins (32, 55).

Glycosylation and functional expression of AeKCC1-A. As shown in Fig. 9D, the nonglycosylated AeKCC1-A protein is unable to reach its full transport potential. Thus, as for other SLC12 transporters (i.e., rat NCC and NKCC2) (32, 55), the *N*-glycosylation of AeKCC1-A is required for its functional expression in *Xenopus* oocytes (Fig. 9D). Although we did not determine the specific mechanism by which the transport activity of nonglycosylated AeKCC1-A is reduced, it is unlikely due to a decrease in the amount of AeKCC1-A protein synthesized by the oocytes, because the GFP immunoreactivities exhibited by AeKCC1-A-eGFP oocytes injected with tunicamycin are similar in intensity to those injected with DMSO (Fig. 9C). A more likely explanation(s) is that *N*-glycosylation of AeKCC1-A 1) facilitates its insertion and/or trafficking into the plasma membrane and/or 2) modulates its binding of and/or affinity for Cl⁻; both the former and latter have been shown to be the case for rat NCC and NKCC2 (32, 55).

AeKCC1 Plays a Central Role in Malpighian Tubule Function

AeKCC1 is an apical K_{Cl} cotransporter. The localization of AeKCC1 immunoreactivity is highly polarized within principal cells, as indicated by the distinct labeling of the luminal brush border (Fig. 11). To our knowledge, this is the first immunolocalization of a SLC12-like transporter in any insect Malpighian tubule. By integrating the localization data with the functional characterization of AeKCC1-A in *Xenopus* oocytes (see above),

we can infer that AeKCC1 mediates a DIOA-sensitive transport of K⁺ and Cl⁻ across the apical membrane of principal cells that is enhanced by cell swelling (see APPENDIX).

Our finding of an apical KCC in the mosquito Malpighian tubule is consistent with the proposition of Whittembury's laboratory that a DIOA-sensitive KCC resides in the luminal membrane of Malpighian tubules of the hemipteran *Rhodnius prolixus* (24). Moreover, our localization results in *Aedes* Malpighian tubules are consistent with the general observations of Zeuthen's laboratory that KCCs are often located at the exit membrane of epithelia that mediate the isosmotic transepithelial transport of fluid, such as the basolateral membrane of vertebrate renal proximal tubules and the apical membrane of the vertebrate choroid plexus (43, 87).

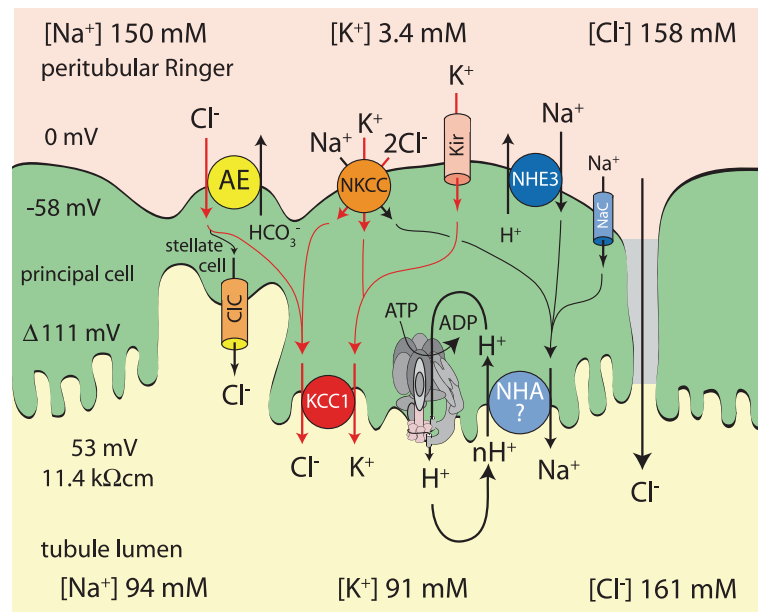
AeKCC1 contributes to the electroneutral transepithelial secretion of fluid by isolated Malpighian tubules. Remarkably, DIOA prominently blocks the transepithelial secretion of fluid by isolated *Aedes* Malpighian tubules (Fig. 12) without significant effects on the electrophysiological parameters of principal cells (Tables 4 and 5). These findings indicate that AeKCC1 plays an integral role in the physiological pathway mediating the electroneutral, transepithelial secretion of fluid in *Aedes* Malpighian tubules, which we have described in previous studies (45, 69).

Putative Role of AeKCC1 in Transepithelial Fluid Secretion

It is now widely appreciated that in epithelia mediating isosmotic, transepithelial fluid transport, the regulation of cell volume by KCCs is functionally linked to the transepithelial movements of salts and water (30, 43). In *Aedes* Malpighian tubules, the apical AeKCC1 of principal cells may also couple cell volume regulation and transepithelial fluid secretion. As shown in Fig. 13, the basal membrane of principal cells is populated by several mechanisms for the entry of peritubular K⁺, Na⁺, and Cl⁻ into the cell. Peritubular Cl⁻ that enters stellate cells via a Cl/HCO₃ anion exchanger may also reach principal cells via gap junctions (82). The entry of electrolytes across basal membranes of the epithelium threatens to increase intracellular osmolarity and cell volume unless the electrolytes are exported again to maintain a steady state. Figure 13 depicts AeKCC1 serving this critical function by mediating the apical extrusion of K⁺ and Cl⁻, thereby maintaining cell volume regulation while also contributing to the transepithelial secretion of fluid.

The above hypothesis is consistent with the properties of AeKCC1-A expressed heterologously in *Xenopus* oocytes and with the effects of DIOA on transepithelial fluid secretion in isolated Malpighian tubules. In the oocyte, AeKCC1-A mediates K_{Cl} symport that is activated by cell swelling (Fig. 7B). In the isolated Malpighian tubule, DIOA significantly reduces rates of transepithelial fluid secretion under control (unstimulated) conditions and in tubules stimulated with the diuretic agents AKIII and db-cAMP (Fig. 12). AKIII activates electrogenic Cl⁻ transport (54, 69), whereas db-cAMP activates electrogenic Na⁺ transport (68, 84, 85). The inhibition of fluid secretion by DIOA under all conditions, without affecting the electrophysiological parameters of the tubule (Tables 4 and 5), may reflect the inhibition of the electroneutral mechanism of fluid secretion that is mediated by AeKCC1 and independent of electrogenic mechanisms.

Fig. 13. Molecular model of transepithelial KCl and NaCl secretion across the Malpighian tubule of *Aedes aegypti*. Modified from Beyenbach et al. (7). The present study reveals the presence of a KCC in the luminal brush border of principal cells where it is hypothesized to mediate a pathway for the electroneutral, transcellular secretion of KCl (red arrows). Known mechanisms for the uptake of ions are shown: AE, Cl/HCO₃ anion exchanger (61); Kir, inward-rectifying K⁺ channel (4, 70); NHE3, Na/H exchanger 3 (64); NKCC, Na,K,2Cl cotransporter (27, 70); NaC, Na⁺-channel (4, 68). Known and putative mechanisms for the secretion of ions are also shown: CIC, Cl⁻ channel (53); NHA (hypothesized), Na/H antiporter; paracellular pathway (54); V-type H⁺-ATPase (81). The electrophysiological data are from Williams and Beyenbach (85); the ionic composition of the luminal fluid is from Williams and Beyenbach (84).



AeKCC1 might also be physically and/or functionally coupled to other transport systems for Na⁺ and Cl⁻. Our laboratory has previously observed evidence for the functional coupling of secretory K⁺, Na⁺, and Cl⁻ transport pathways in *Aedes* Malpighian tubules (27, 70). Moreover, recent studies in vertebrate epithelia and heterologous expression systems have revealed that KCCs can form physical and functional associations with other KCCs, NKCCs, and ATPases (18, 19, 35, 71). Similar associations among *AeKCC1* and other transporters of electrolytes may also contribute to the inhibition of fluid secretion by DIOA in isolated Malpighian tubules.

Perspectives and Significance

The present study demonstrates that the luminal membrane of principal cells in *Aedes* Malpighian tubules expresses a SLC12-like, DIOA-sensitive KCC (*AeKCC1-A*). In view of the dramatic inhibitory effects of DIOA on the renal tubule output of mosquitoes under both control and diuretic conditions, without effecting the electrophysiological parameters of the epithelium, *AeKCC1-A* appears to be the molecular cornerstone of an enigmatic electroneutral mechanism for the transepithelial secretion of fluid by Malpighian tubules that we have observed before in this highly electrogenic epithelium (45, 69). Furthermore, our present study on mosquito Malpighian tubules 1) supports the pioneering work Gutierrez et al. (24), which was the first to propose the hypothesis of an apical KCC in insect Malpighian tubules and 2) warrants further investigations into the potential roles of KCCs in Malpighian tubule function of other insects, especially in those of insects for which DIOA has been shown to prominently block fluid secretion, such as in *D. melanogaster* (42).

APPENDIX

Below we examine the thermodynamics of K,Cl cotransport across the apical membrane of principal cells. For an electroneutral cotransporter such as a KCC, the direction of transport depends on the net chemical potential according to Eq. 1, which can also be expressed as Eq. 2.

$$\mu_{c_{K^+}} = -\mu_{c_{Cl^-}} \quad (1)$$

$$RT\ln\frac{[K^+]_{cell}}{[K^+]_{lumen}} = -RT\ln\frac{[Cl^-]_{cell}}{[Cl^-]_{lumen}} \quad (2)$$

where R is gas constant, T is temperature, and ln is natural logarithm. For an apical KCC, Eq. 2 reduces to Eq. 3:

$$[K^+]_{cell}[Cl^-]_{cell} = [K^+]_{lumen}[Cl^-]_{lumen} \quad (3)$$

In *Aedes* Malpighian tubules, under control conditions of fluid secretion, the concentrations of K⁺ and Cl⁻ in the tubule lumen are, respectively, 91 mM and 161 mM (84). Measurements of intracellular Cl⁻ concentrations by our laboratory (using 2 independent methods) indicate high-cytoplasmic Cl⁻ concentrations of ~125 mM in principal cells of *Aedes* Malpighian tubules (unpublished observations). According to Eq. 3, the intracellular K⁺ concentration must therefore be ~120 mM to allow for KCC-mediated K,Cl export across the apical membrane into the tubule lumen. Intracellular K⁺ concentrations of 120 mM are within the normal physiological range of eukaryotic cells, and values as high as 123 mM have been recorded in principal cells of *Aedes* Malpighian tubules (58). Accordingly, KCC-mediated export across the apical membrane of principal cells in *Aedes* Malpighian tubules appears feasible on thermodynamic grounds. This notion becomes even more feasible when one considers that K⁺ and Cl⁻ can accumulate disproportionately to the apical cytoplasm of principal cells (vs. the intermediate and basal cytoplasm) in Malpighian tubules of at least one dipteran *D. hydei* (83).

ACKNOWLEDGMENTS

We thank the laboratory of William A. Horne (Clinical Sciences) at the Cornell University College of Veterinary Medicine for generously supplying the oocytes used in this study. We are also indebted to the laboratory of Michael I. Kotlikoff (Cornell University College of Veterinary Medicine) for providing equipment used in Western blot analysis. Finally, we thank Longying Dong, Mary Lou Norman, and Jeff Leavey (all of Cornell University) for their excellent technical assistance.

GRANTS

Financial support for this study was from National Institute of Diabetes and Digestive and Kidney Diseases Grant K01-DK-080194-01 (to P. M. Piermarini) and National Science Foundation Grant IBN-0078058 (to K. W. Beyenbach). The contributions of R. M. Hine were in part supported by a 2009

ARRA National Institutes of Health Administrative Supplement (to P. M. Piermarini).

DISCLOSURES

No conflicts of interest, financial or otherwise, are declared by the author(s).

REFERENCES

- Adragna NC, Fulvio MD, Lauf PK. Regulation of K-Cl cotransport: from function to genes. *J Membr Biol* 201: 109–137, 2004.
- Bankfalvi A, Navabi H, Bier B, Bocker W, Jasani B, Schmid KW. Wet autoclave pretreatment for antigen retrieval in diagnostic immunohistochemistry. *J Pathol* 174: 223–228, 1994.
- Heyenbach KW. Transport mechanisms of diuresis in Malpighian tubules of insects. *J Exp Biol* 206: 3845–3856, 2003.
- Heyenbach KW, Masia R. Membrane conductances of principal cells in Malpighian tubules of *Aedes aegypti*. *J Insect Physiol* 48: 375–386, 2002.
- Heyenbach KW, Piermarini PM. Osmotic and ionic regulation in insects. In: *Osmotic and Ionic Regulation: Cells and Animals*, edited by Evans DH. Boca Raton, FL: CRC, 2009, p. 231–293.
- Heyenbach KW, Piermarini PM. Transcellular and paracellular pathways of transepithelial fluid secretion in Malpighian (renal) tubules of the yellow fever mosquito *Aedes aegypti*. *Acta Physiol* 202: 387–407, 2010.
- Heyenbach KW, Skaer H, Dow JA. The developmental, molecular, and transport biology of Malpighian tubules. *Annu Rev Entomol* 55: 351–374, 2010.
- Blom N, Gammeltoft S, Brunak S. Sequence and structure-based prediction of eukaryotic protein phosphorylation sites. *J Mol Biol* 294: 1351–1362, 1999.
- Boettger T, Hubner CA, Maier H, Rust MB, Beck FX, Jentsch TJ. Deafness and renal tubular acidosis in mice lacking the K-Cl co-transporter Kcc4. *Nature* 416: 874–878, 2002.
- Casula S, Shmukler BE, Wilhelm S, Stuart-Tilley AK, Su W, Chernova MN, Brugnara C, Alper SL. A dominant negative mutant of the KCC1 K-Cl cotransporter: both N- and C-terminal cytoplasmic domains are required for K-Cl cotransport activity. *J Biol Chem* 276: 41870–41878, 2001.
- Chatterjee S, Pal JK. Role of 5'- and 3'-untranslated regions of mRNAs in human diseases. *Biol Cell* 101: 251–262, 2009.
- Clements AN. *The Biology of Mosquitoes*. London: Chapman and Hall, 1992.
- Coast GM, Garside CS, Webster SG, Schegg KM, Schooley DA. Mosquito natriuretic peptide identified as a calcitonin-like diuretic hormone in *Anopheles gambiae* (Giles). *J Exp Biol* 208: 3281–3291, 2005.
- Combet C, Blanchet C, Geourjon C, Deleage G. NPS@: network protein sequence analysis. *Trends Biochem Sci* 25: 147–150, 2000.
- de Los Heros P, Kahle KT, Rinehart J, Bobadilla NA, Vazquez N, San Cristobal P, Mount DB, Lifton RP, Hebert SC, Gamba G. WNK3 bypasses the tonicity requirement for K-Cl cotransporter activation via a phosphatase-dependent pathway. *Proc Natl Acad Sci USA* 103: 1976–1981, 2006.
- Fujii T, Fujita K, Shimizu T, Takeguchi N, Sakai H. The NH₂-terminus of K⁺-Cl⁻ cotransporter 3a is essential for up-regulation of Na⁺, K⁺-ATPase activity. *Biochem Biophys Res Commun* 399: 683–687, 2010.
- Fujii T, Ohira Y, Itomi Y, Takahashi Y, Asano S, Morii M, Takeguchi N, Sakai H. Inhibition of P-type ATPases by dihydroindolenyl(oxy)acetic acid (DIOA), a K⁺-Cl⁻ cotransporter inhibitor. *Eur J Pharmacol* 560: 123–126, 2007.
- Fujii T, Takahashi Y, Ikari A, Morii M, Tabuchi Y, Tsukada K, Takeguchi N, Sakai H. Functional association between K⁺-Cl⁻ cotransporter-4 and H⁺, K⁺-ATPase in the apical canalicular membrane of gastric parietal cells. *J Biol Chem* 284: 619–629, 2009.
- Fujii T, Takahashi Y, Itomi Y, Fujita K, Morii M, Tabuchi Y, Asano S, Tsukada K, Takeguchi N, Sakai H. K⁺-Cl⁻ cotransporter-3a up-regulates Na⁺, K⁺-ATPase in lipid rafts of gastric luminal parietal cells. *J Biol Chem* 283: 6869–6877, 2008.
- Gagnon KB, England R, Delpire E. Volume sensitivity of cation-Cl⁻ cotransporters is modulated by the interaction of two kinases: Ste20-related proline-alanine-rich kinase and WNK4. *Am J Physiol Cell Physiol* 290: C134–C142, 2006.
- Gamba G. Molecular physiology and pathophysiology of electroneutral cation-chloride cotransporters. *Physiol Rev* 85: 423–493, 2005.
- Garzon-Muñoz T, Pacheco-Alvarez D, Gagnon KB, Vazquez N, Ponce-Coria J, Moreno E, Delpire E, Gamba G. WNK4 kinase is a negative regulator of K⁺-Cl⁻ cotransporters. *Am J Physiol Renal Physiol* 292: F1197–F1207, 2007.
- Gillen CM, Brill S, Payne JA, Forbush B 3rd. Molecular cloning and functional expression of the K-Cl cotransporter from rabbit, rat, and human. A new member of the cation-chloride cotransporter family. *J Biol Chem* 271: 16237–16244, 1996.
- Gutierrez AM, Hernandez CS, Whittembury G. A model for fluid secretion in *Rhodnius* upper Malpighian tubules (UMT). *J Membr Biol* 202: 105–114, 2004.
- Hall TA. BioEdit: a user-friendly biological sequence alignment editor and analysis program for Windows 95/98/NT. *Nucl Acids Symp Ser* 41: 95–98, 1999.
- Hebert SC, Mount DB, Gamba G. Molecular physiology of cation-coupled Cl⁻ cotransport: the SLC12 family. *Pflügers Arch* 447: 580–593, 2004.
- Hegarty JL, Zhang B, Pannabecker TL, Petzel DH, Baustian MD, Heyenbach KW. Dibutyryl cAMP activates bumetanide-sensitive electrolyte transport in Malpighian tubules. *Am J Physiol Cell Physiol* 261: C521–C529, 1991.
- Hekmat-Scafe DS, Lundy MY, Ranga R, Tanouye MA. Mutations in the K⁺/Cl⁻ cotransporter gene kazachoc (kcc) increase seizure susceptibility in *Drosophila*. *J Neurosci* 26: 8943–8954, 2006.
- Hekmat-Scafe DS, Mercado A, Fajilan AA, Lee AW, Hsu R, Mount DB, Tanouye MA. Seizure sensitivity is ameliorated by targeted expression of K⁺-Cl⁻ cotransporter function in the mushroom body of the *Drosophila* brain. *Genetics* 184: 171–183, 2010.
- Hoffmann EK, Lambert IH, Pedersen SF. Physiology of cell volume regulation in vertebrates. *Physiol Rev* 89: 193–277, 2009.
- Holtzman EJ, Kumar S, Faaland CA, Warner F, Logue PJ, Erickson SJ, Ricken G, Waldman J, Dunham PB. Cloning, characterization, and gene organization of K-Cl cotransporter from pig and human kidney and *C. elegans*. *Am J Physiol Renal Physiol* 275: F550–F564, 1998.
- Hoover RS, Poch E, Monroy A, Vazquez N, Nishio T, Gamba G, Hebert SC. N-glycosylation at two sites critically alters thiazide binding and activity of the rat thiazide-sensitive Na⁺:Cl⁻ cotransporter. *J Am Soc Nephrol* 14: 271–282, 2003.
- Ianowski JP, O'Donnell MJ. Basolateral ion transport mechanisms during fluid secretion by *Drosophila* Malpighian tubules: Na⁺ recycling, Na⁺:K⁺:2 Cl⁻ cotransport and Cl⁻ conductance. *J Exp Biol* 207: 2599–2609, 2004.
- Ianowski JP, O'Donnell MJ. Electrochemical gradients for Na⁺, K⁺, Cl⁻ and H⁺ across the apical membrane in Malpighian (renal) tubule cells of *Rhodnius prolixus*. *J Exp Biol* 209: 1964–1975, 2006.
- Ikeda K, Onimaru H, Yamada J, Inoue K, Ueno S, Onaka T, Toyoda H, Arata A, Ishikawa TO, Taketo MM, Fukuda A, Kawakami K. Malfunction of respiratory-related neuronal activity in Na⁺, K⁺-ATPase-α₂ subunit-deficient mice is attributable to abnormal Cl⁻ homeostasis in brainstem neurons. *J Neurosci* 24: 10693–10701, 2004.
- Jentsch TJ. Chloride transport in the kidney: lessons from human disease and knockout mice. *J Am Soc Nephrol* 16: 1549–1561, 2005.
- Kahle KT, Rinehart J, Lifton RP. Phosphoregulation of the Na-K-Cl and K-Cl cotransporters by the WNK kinases. *Biochim Biophys Acta* 1802: 1150–1158, 2010.
- Laemmli UK. Cleavage of structural proteins during assembly of the head of bacteriophage T4. *Nature* 227: 680–685, 1970.
- Larkin MA, Blackshields G, Brown NP, Chenna R, McGettigan PA, McWilliam H, Valentin F, Wallace IM, Wilm A, Lopez R, Thompson JD, Gibson TJ, Higgins DG. ClustalW and ClustalX version 2. *Bioinformatics* 23: 2947–2948, 2007.
- Lauf PK, Adragna NC. K-Cl cotransport: properties and molecular mechanism. *Cell Physiol Biochem* 10: 341–354, 2000.
- Leysens A, Dijkstra S, Van Kerckhove E, Steels P. Mechanisms of K⁺ uptake across the basal membrane of Malpighian tubules of *Formica polyctena*: the effect of ions and inhibitors. *J Exp Biol* 195: 123–145, 1994.
- Linton SM, O'Donnell MJ. Contributions of K⁺:Cl⁻ cotransport and Na⁺/K⁺-ATPase to basolateral ion transport in malpighian tubules of *Drosophila melanogaster*. *J Exp Biol* 202: 1561–1570, 1999.
- MacAulay N, Hamann S, Zeuthen T. Chloride transporters as water pumps: elements in a new model of epithelial water transport. In: *Physiology and Pathology of Chloride Transporters and Channels in the Nervous System*, edited by Alvarez-Leefmans FJ and Delpire E. London: Elsevier, 2009, p. 547–568.

44. **Masia R, Aneshansley D, Nagel W, Nachman RJ, Beyenbach KW.** Voltage clamping single cells in intact Malpighian tubules of mosquitoes. *Am J Physiol Renal Physiol* 279: F747–F754, 2000.
45. **Massaro RC, Lee LW, Patel AB, Wu DS, Yu MJ, Scott BN, Schooley DA, Schegg KM, Beyenbach KW.** The mechanism of action of the antidiuretic peptide Tenmo ADFa in Malpighian tubules of *Aedes aegypti*. *J Exp Biol* 207: 2877–2888, 2004.
46. **Mercado A, Broumand V, Zandi-Nejad K, Enck AH, Mount DB, Gamba G.** Functional and molecular characterization of the K-Cl cotransporter of *Xenopus laevis* oocytes. *Am J Physiol Cell Physiol* 281: C670–C680, 2001.
47. **Mercado A, de los Heros P, Vazquez N, Meade P, Mount DB, Gamba G.** Functional comparison of the K⁺-Cl⁻ cotransporters KCC1 and KCC4. *J Biol Chem* 275: 30326–30334, 2000.
48. **Mercado A, Vazquez N, Song L, Cortes R, Enck AH, Welch R, Delpire E, Gamba G, Mount DB.** NH₂-terminal heterogeneity in the KCC3 K⁺-Cl⁻ cotransporter. *Am J Physiol Renal Physiol* 289: F1246–F1261, 2005.
49. **Mount DB, Mercado A, Song L, Xu J, George AL Jr, Delpire E, Gamba G.** Cloning and characterization of KCC3 and KCC4, new members of the cation-chloride cotransporter gene family. *J Biol Chem* 274: 16355–16362, 1999.
50. **Nazeer K, Janech MG, Lin JJ, Ryan KJ, Arthur JM, Budisavljevic MN.** Changes in protein profiles during course of experimental glomerulonephritis. *Am J Physiol Renal Physiol* 296: F186–F193, 2009.
51. **Nene V, Wortman JR, Lawson D, Haas B, Kodira C, Tu ZJ, Loftus B, Xi Z, Megy K, Grabherr M, Ren Q, Zdobnov EM, Lobo NF, Campbell KS, Brown SE, Bonaldo MF, Zhu J, Sinkins SP, Hogenkamp DG, Amedeo P, Arensburger P, Atkinson PW, Bidwell S, Biedler J, Birney E, Bruggner RV, Costas J, Coy MR, Crabtree J, Crawford M, Debruyne B, Decaprio D, Eiglmeier K, Eisenstadt E, El-Dorry H, Gelbart WM, Gomes SL, Hammond M, Hannick LI, Hogan JR, Holmes MH, Jaffe D, Johnston JS, Kennedy RC, Koo H, Kravitz S, Kriventseva EV, Kulp D, Labutti K, Lee E, Li S, Lovin DD, Mao C, Mauceli E, Menek CF, Miller JR, Montgomery P, Mori A, Nascimento AL, Naveira HF, Nusbaum C, O'Leary S, Orvis J, Pertea M, Quesneville H, Reidenbach KR, Rogers YH, Roth CW, Schneider JR, Schatz M, Shumway M, Stanke M, Stinson EO, Tubio JM, Vanzeer JP, Verjovski-Almeida S, Werner D, White O, Wyder S, Zeng Q, Zhao Q, Zhao Y, Hill CA, Raikhel AS, Soares MB, Knudson DL, Lee NH, Galagan J, Salzberg SL, Paulsen IT, Dimopoulos G, Collins FH, Birren B, Fraser-Liggett CM, Severson DW.** Genome sequence of *Aedes aegypti*, a major arbovirus vector. *Science* 316: 1718–1723, 2007.
52. **O'Connor KR, Beyenbach KW.** Chloride channels in apical membrane patches of stellate cells of Malpighian tubules of *Aedes aegypti*. *J Exp Biol* 204: 367–378, 2001.
53. **Pannabecker TL, Hayes TK, Beyenbach KW.** Regulation of epithelial shunt conductance by the peptide leucokinin. *J Membr Biol* 132: 63–76, 1993.
54. **Paredes A, Plata C, Rivera M, Moreno E, Vazquez N, Munoz-Clares R, Hebert SC, Gamba G.** Activity of the renal Na⁺-K⁺-2 Cl⁻ cotransporter is reduced by mutagenesis of N-glycosylation sites: role for protein surface charge in Cl⁻ transport. *Am J Physiol Renal Physiol* 290: F1094–F1102, 2006.
55. **Payne JA.** Functional characterization of the neuronal-specific K-Cl cotransporter: implications for [K⁺]_o regulation. *Am J Physiol Cell Physiol* 273: C1516–C1525, 1997.
56. **Payne JA, Stevenson TJ, Donaldson LF.** Molecular characterization of a putative K-Cl cotransporter in rat brain. A neuronal-specific isoform. *J Biol Chem* 271: 16245–16252, 1996.
57. **Petzel DH, Pirotte PT, Van Kerckhove E.** Intracellular and luminal pH measurements of Malpighian tubules of the mosquito *Aedes aegypti*: the effects of cAMP. *J Insect Physiol* 45: 973–982, 1999.
58. **Pickering BM, Willis AE.** The implications of structured 5' untranslated regions on translation and disease. *Semin Cell Dev Biol* 16: 39–47, 2005.
59. **Piechotta K, Lu J, Delpire E.** Cation chloride cotransporters interact with the stress-related kinases Ste20-related proline-alanine-rich kinase (SPAK) and oxidative stress response 1 (OSR1). *J Biol Chem* 277: 50812–50819, 2002.
60. **Piermarini PM, Grogan LF, Lau K, Wang L, Beyenbach KW.** A SLC4-like anion exchanger from renal tubules of the mosquito (*Aedes aegypti*): evidence for a novel role of stellate cells in diuretic fluid secretion. *Am J Physiol Regul Integr Comp Physiol* 298: R642–R660, 2010.
61. **Piermarini PM, Weihrauch D, Meyer H, Huss M, Beyenbach KW.** NHE8 is an intracellular cation/H⁺ exchanger in renal tubules of the yellow fever mosquito *Aedes aegypti*. *Am J Physiol Renal Physiol* 296: F730–F750, 2009.
62. **Pond BB, Galeffi F, Ahrens R, Schwartz-Bloom RD.** Chloride transport inhibitors influence recovery from oxygen-glucose deprivation-induced cellular injury in adult hippocampus. *Neuropharmacology* 47: 253–262, 2004.
63. **Pullikuth AK, Aimanova K, Kang'ethe W, Sanders HR, Gill SS.** Molecular characterization of sodium/proton exchanger 3 (NHE3) from the yellow fever vector, *Aedes aegypti*. *J Exp Biol* 209: 3529–3544, 2006.
64. **Ramsay JA.** Active transport of potassium by the Malpighian tubules of insects. *J Exp Biol* 93: 358–369, 1953.
65. **Rinehart J, Maksimova YD, Tanis JE, Stone KL, Hodson CA, Zhang J, Risinger M, Pan W, Wu D, Colangelo CM, Forbush B, Joiner CH, Gulcicek EE, Gallagher PG, Lifton RP.** Sites of regulated phosphorylation that control K-Cl cotransporter activity. *Cell* 138: 525–536, 2009.
66. **Roitberg BD, Mondor EB, Tyerman JGA.** Pouncing spider, flying mosquito: blood acquisition increases predation risk in mosquitoes. *Behav Ecol* 14: 736–740, 2003.
67. **Sawyer DB, Beyenbach KW.** Dibutyryl-cAMP increases basolateral sodium conductance of mosquito Malpighian tubules. *Am J Physiol Regul Integr Comp Physiol* 248: R339–R345, 1985.
68. **Schepel SA, Fox AJ, Miyauchi JT, Sou T, Yang JD, Lau K, Blum AW, Nicholson LK, Tiburey F, Nachman RJ, Piermarini PM, Beyenbach KW.** The single kinin receptor signals to separate and independent physiological pathways in Malpighian tubules of the yellow fever mosquito. *Am J Physiol Regul Integr Comp Physiol* 299: R612–R622, 2010.
69. **Scott BN, Yu MJ, Lee LW, Beyenbach KW.** Mechanisms of K⁺ transport across basolateral membranes of principal cells in Malpighian tubules of the yellow fever mosquito, *Aedes aegypti*. *J Exp Biol* 207: 1655–1663, 2004.
70. **Simard CF, Bergeron MJ, Frenette-Cotton R, Carpentier GA, Pelchat ME, Caron L, Isenring P.** Homooligomeric and heterooligomeric associations between K⁺-Cl⁻ cotransporter isoforms and between K⁺-Cl⁻ and Na⁺-K⁺-Cl⁻ cotransporters. *J Biol Chem* 282: 18083–18093, 2007.
71. **Song L, Mercado A, Vazquez N, Xie Q, Desai R, George AL Jr, Gamba G, Mount DB.** Molecular, functional, and genomic characterization of human KCC2, the neuronal K-Cl cotransporter. *Mol Brain Res* 103: 91–105, 2002.
72. **Strange K, Singer TD, Morrison R, Delpire E.** Dependence of KCC2 K-Cl cotransporter activity on a conserved carboxy terminus tyrosine residue. *Am J Physiol Cell Physiol* 279: C860–C867, 2000.
73. **Su W, Shmukler BE, Chernova MN, Stuart-Tilley AK, de Franceschi L, Brugnara C, Alper SL.** Mouse K-Cl cotransporter KCC1: cloning, mapping, pathological expression, and functional regulation. *Am J Physiol Cell Physiol* 277: C899–C912, 1999.
74. **Sun Q, Tian E, Turner RJ, Ten Hagen KG.** Developmental and functional studies of the SLC12 gene family members from *Drosophila melanogaster*. *Am J Physiol Cell Physiol* 298: C26–C37, 2010.
75. **Tamura K, Dudley J, Nei M, Kumar S.** MEGA4: Molecular Evolutionary Genetics Analysis (MEGA) software version 4.0. *Mol Biol Evol* 24: 1596–1599, 2007.
76. **Tanis JE, Bellemere A, Moresco JJ, Forbush B, Koelle MR.** The potassium chloride cotransporter KCC-2 coordinates development of inhibitory neurotransmission and synapse structure in *Caenorhabditis elegans*. *J Neurosci* 29: 9943–9954, 2009.
77. **Trudeau MC, Warmke JW, Ganetzky B, Robertson GA.** HERG, a human inward rectifier in the voltage-gated potassium channel family. *Science* 269: 92–95, 1995.
78. **Uvarov P, Ludwig A, Markkanen M, Pruunsild P, Kaila K, Delpire E, Timmusk T, Rivera C, Airaksinen MS.** A novel N-terminal isoform of the neuron-specific K-Cl cotransporter KCC2. *J Biol Chem* 282: 30570–30576, 2007.
79. **Velez JC, Bland AM, Arthur JM, Raymond JR, Janech MG.** Characterization of renin-angiotensin system enzyme activities in cultured mouse podocytes. *Am J Physiol Renal Physiol* 293: F398–F407, 2007.

81. Weng XH, Huss M, Wieczorek H, Beyenbach KW. The V-type H^+ -ATPase in Malpighian tubules of *Aedes aegypti*: localization and activity. *J Exp Biol* 206: 2211–2219, 2003.
82. Weng XH, Piermarini PM, Yamahiro A, Yu MJ, Aneshansley DJ, Beyenbach KW. Gap junctions in Malpighian tubules of *Aedes aegypti*. *J Exp Biol* 211: 409–422, 2008.
83. Wessing A, Zierold K. Heterogeneous distribution of elemental contents in the larval Malpighian tubules of *Drosophila hydei*: X-ray microanalysis of freeze-dried cryosections. *Cell Tissue Res* 272: 491–497, 1993.
84. Williams JC, Beyenbach KW. Differential effects of secretagogues on Na and K secretion in the Malpighian tubules of *Aedes aegypti*. *J Comp Physiol B* 149: 511–518, 1983.
85. Williams JC, Beyenbach KW. Differential effects of secretagogues on the electrophysiology of the Malpighian tubules of the yellow fever mosquito. *J Comp Physiol B* 154: 301–309, 1984.
86. Yu MJ, Beyenbach KW. Leucokinin activates Ca^{2+} -dependent signal pathway in principal cells of *Aedes aegypti* Malpighian tubules. *Am J Physiol Renal Physiol* 283: F499–F508, 2002.
87. Zeuthen T. Water-transporting proteins. *J Membr Biol* 234: 57–73, 2010.
88. Zubrzak P, Williams H, Coast GM, Isaac RE, Reyes-Rangel G, Juaristi E, Zabrocki J, Nachman RJ. β -amino acid analogs of an insect neuropeptide feature potent bioactivity and resistance to peptidase hydrolysis. *Biopolymers* 88: 76–82, 2007.

